First passage in an interval for fractional Brownian motion

Kay Jörg Wiese
Laboratoire de Physique de l'Ecole normale supérieure, ENS, Université PSL, CNRS, Sorbonne Université, Université Paris-Diderot, Sorbonne Paris Cité, Paris, France

(Received 2 August 2018; published 6 March 2019)

Let X_t be a random process starting at $x \in [0,1]$ with absorbing boundary conditions at both ends of the interval. Denote by $P_1(x)$ the probability to first exit at the upper boundary. For Brownian motion, $P_1(x) = x$, which is equivalent to $P_1'(x) = 1$. For fractional Brownian motion with Hurst exponent H, we establish that $P_1'(x) = \mathcal{N}[x(1-x)]^{1/H-2} e^{\epsilon \mathcal{F}(x)+O(\epsilon^2)}$, where $\epsilon = H - \frac{1}{2}$. The function $\mathcal{F}(x)$ is analytic and well approximated by its Taylor expansion $\mathcal{F}(x) \simeq 16(C-1)(x-\frac{1}{2})^2 + O(x-\frac{1}{2})^4$, where $C = 0.915\ldots$ is the Catalan constant. A similar result holds for moments of the exit time starting at x. We then consider the span of X_t, i.e., the size of the (compact) domain visited up to time t. For Brownian motion, we derive an analytic expression for the probability that the span reaches 1 for the first time and then generalize it to fractional Brownian motion. Using large-scale numerical simulations with system sizes up to $N = 2^{24}$ and a broad range of H, we confirm our analytic results. There are important finite-discretization corrections which we quantify. They are most severe for small H, necessitating going to the large systems mentioned above.

DOI: 10.1103/PhysRevE.99.032106

I. INTRODUCTION

A key problem in stochastic processes is the first-passage properties [1,2] in a finite domain, say, the unit interval [0,1]. For Brownian motion, the probability to exit at the upper boundary $x = 1$, starting at x, is

$$P_1^0(x) = x. \tag{1}$$

Another key observable is the exit time, starting at x, which behaves as $\langle T_{\text{exit}}(x)\rangle_0 \sim x(1-x)$. Many physical situations, however, cannot be described by Brownian motion. An example is a polymer translocating through a nanopore. While the motion of the polymer as a whole is a Markov process, the effective process for its position in the pore is non-Markovian [3–8]. The questions posed above become much more involved for the latter. The simplest generalization is fractional Brownian motion (FBM): It is the unique process that retains, from Brownian motion, Gaussianity and scale and translational invariance in both space and time and is drift-free. Fractional Brownian motion was introduced in its final form by Mandelbrot and Van Ness [9]. It is indexed by the Hurst exponent H, with $0 < H \leqslant 1$ (see Fig. 1). As a Gaussian process, it is specified by its second moment

$$\langle X(t_1)X(t_2)\rangle = t_1^{2H} + t_2^{2H} - |t_1 - t_2|^{2H}. \tag{2}$$

Fractional Brownian motion is important as it successfully models a variety of natural processes [13,14]: a tagged particle in single-file diffusion ($H = 0.25$) [15,16], the integrated current in diffusive transport ($H = 0.25$) [17], polymer translocation through a narrow pore ($H \simeq 0.4$) [8,18,19], anomalous diffusion [20], values of the logarithmic return of a stock ($H \simeq 0.6$–0.8) [21,22], hydrology ($H \simeq 0.72$–0.87) [23], a tagged monomer in a polymer ($H = 0.25$) [24], solar flare activity ($H \simeq 0.57$–0.86) [25], the price of electricity in a liberated market ($H \simeq 0.41$) [26], telecommunication networks ($H \simeq 0.78$–0.86) [27], telomeres inside the nucleus of human cells ($H \simeq 0.18$–0.35) [28], or diffusion inside crowded fluids ($H \simeq 0.4$) [29].

There are yet no analytical methods to treat the questions posed above for H other than $1/2$ (Brownian motion) and $H = 1$ (a straight line with a random slope). To remedy this, we developed tools [30–35] which allow us to answer this question analytically, in a Taylor expansion around $H = 1/2$, i.e., in

$$\epsilon = H - \tfrac{1}{2}. \tag{3}$$

These methods have proven feasible and precise up to second order in ϵ [36], where they allowed us to distinguish the three classical arcsine laws. In this article we generalize the exit probability and distribution of exit times to fractional Brownian motion (Fig. 1). It had earlier been argued [37] that the exit probability at the upper boundary scales for small x as

$$P_1(x) \sim x^{\phi}, \quad \phi = \frac{\theta}{H}, \tag{4}$$

where θ is the persistence exponent. For FBM [30,38]

$$\theta = 1 - H. \tag{5}$$

This led the authors of Ref. [37] to conjecture that $P_1'(x) \sim [x(1-x)]^{1/H-2}$ for all x. This however is too simple an approximation [37]. Here we show analytically that $P_1'(x)$ can be written in the form

$$P_1'(x) = \mathcal{N}[x(1-x)]^{1/H-2} e^{\epsilon \mathcal{F}(x)+O(\epsilon^2)}, \tag{6}$$

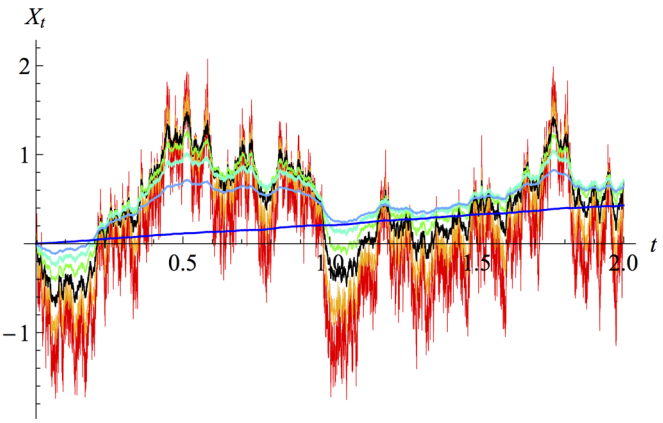

FIG. 1. Realizations of a FBM for $H = 0.25$ (red, roughest curve); $H = 0.375$ (orange); $H = 1/2$, Brownian (black); $H = 0.625$ (green); $H = 0.75$ (cyan); $H = 0.875$ (bright blue); and $H = 1$ (dark blue, straight line), using the algorithm of Davies and Harte [10–12].

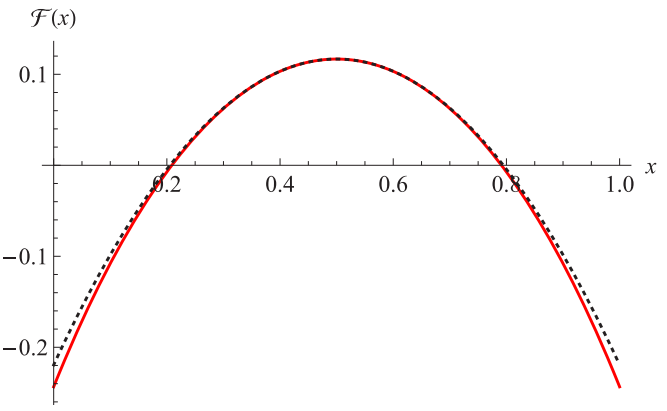

FIG. 2. Scaling function $\mathcal{F}(x)$ defined in Eq. (72) (solid red curve), normalized such that $\int_0^1 \mathcal{F}(x)dx = 0$. The dashed line is the quadratic term given in Eq. (8).

where $\mathcal{F}(x)$ is an analytic function

$$\mathcal{F}(x) = 4\Big[12\zeta'(-1) + \frac{\ln(2)}{3} + \ln(x(1-x)) + \ln\left(\Gamma\left(\frac{1}{2} - \frac{x}{2}\right)\right) - \ln\left(\Gamma\left(1 - \frac{x}{2}\right)\right) + \ln\left(\Gamma\left(\frac{x}{2}\right)\right) - \ln\left(\Gamma\left(\frac{x+1}{2}\right)\right)\Big]. \quad (7)$$

Absorbing the constant into the normalization $\mathcal{N}$, its Taylor expansion reads

$$\begin{aligned}\mathcal{F}(x) &= 4 - \tfrac{20}{3}\ln(2) + 8\big[\ln\left(\Gamma\left(\tfrac{1}{4}\right)\right) - \ln\left(\Gamma\left(\tfrac{3}{4}\right)\right) + 6\zeta'(-1)\big] \\ &\quad + 16(C-1)\big(x-\tfrac{1}{2}\big)^2 + \tfrac{1}{48}\big(x-\tfrac{1}{2}\big)^4 \\ &\quad \times \big[\psi^{(3)}\big(\tfrac{1}{4}\big) - \psi^{(3)}\big(\tfrac{3}{4}\big) - 1536\big] + O\big(x-\tfrac{1}{2}\big)^6 \\ &= 0.116\,736 - 1.344\,55\big(x-\tfrac{1}{2}\big)^2 \\ &\quad - 0.353\,774\big(x-\tfrac{1}{2}\big)^4 + O\big(x-\tfrac{1}{2}\big)^6. \end{aligned} \quad (8)$$

The number C is the Catalan constant

$$C = \sum_{n=0}^{\infty} \frac{(-1)^n}{(2n+1)^2} \approx 0.915\,965\,594\ldots \quad (9)$$

and $\psi^{(3)}(x) = \partial_x^4 \ln(\Gamma(x))$ the polygamma function of order 3. As can be seen in Fig. 2, the function $\mathcal{F}(x)$ is well approximated by its second Taylor coefficient. Incorporating the fourth-order term, the analytic result and Taylor expansion are indistinguishable on this plot. As a consequence, the most relevant information is captured by the curvature of $\mathcal{F}(x)$ at $x = 1/2$,

$$\gamma := \tfrac{1}{2}\mathcal{F}''(x)|_{x=1/2} = 16(C-1). \quad (10)$$

We believe that higher-order terms in ϵ entering into the exponential of Eq. (6) are also analytic and well approximated by their low-order (in x) Taylor coefficients. We can therefore ask how the effective curvature γ, defined by the first equality in Eq. (10), changes with H. The answer can be read off from Fig. 3: Consider the top (blue) data in Fig. 3(a), obtained for the largest systems. One can see that γ depends on H and that for $H \to \frac{1}{2}$ it extrapolates to $\gamma = -1.34 \pm 0.02$, in agreement with the analytical result (8).

This article is organized as follows. We first derive key results for Brownian motion in Sec. II. Most of them are known [1,2], except for the span observables. After a short review of the ϵ expansion in Sec. III, we derive in Sec. IV the leading-order corrections for FBM for a number of key observables. All our results are checked via extensive numerical simulations in Sec. V. We summarize in Sec. VI.

II. BASIC FORMULAS FOR BROWNIAN MOTION WITH TWO ABSORBING BOUNDARIES

A. Solving the Fokker-Planck equation

Brownian motion from x to y in time t satisfies the forward Fokker-Planck equation [1,2]

$$\partial_t P_+(x,y,t) = \partial_y^2 P_+(x,y,t). \quad (11)$$

The plus refers to surviving paths. Its general solution with absorbing walls at $x = 0$ and $x = 1$ can be written as

$$\begin{aligned} P_+(x,y,t) &= \frac{1}{\sqrt{4\pi t}} \sum_{n=-\infty}^{\infty} \left(e^{-(x-y+2n)^2/4t} - e^{-(x+y+2n)^2/4t}\right) \\ &= \frac{1}{2}\vartheta_3\left(\frac{\pi}{2}(x-y), e^{-\pi^2 t}\right) - \frac{1}{2}\vartheta_3\left(\frac{\pi}{2}(x+y), e^{-\pi^2 t}\right), \end{aligned} \quad (12)$$

where ϑ is the elliptic ϑ function. To prove this statement it is enough to remark that the first line satisfies the Fokker-Planck equation (11), vanishes at $y = 0$ and $y = 1$, and reduces for $t \to 0$ to a δ function

$$\lim_{t\to 0} P_+(x,y,t) = \delta(x-y). \quad (13)$$

Let us introduce the notation

$$\mathbb{P}(z,t) := \frac{1}{\sqrt{4\pi t}} \sum_{n=-\infty}^{\infty} e^{-(z+2n)^2/4t} = \frac{1}{2}\vartheta_3\left(\frac{\pi}{2}z, e^{-\pi^2 t}\right). \quad (14)$$

In terms of this function, Eq. (12) can be written as

$$P_+(x,y,t) = \mathbb{P}(x-y,t) - \mathbb{P}(x+y,t). \quad (15)$$

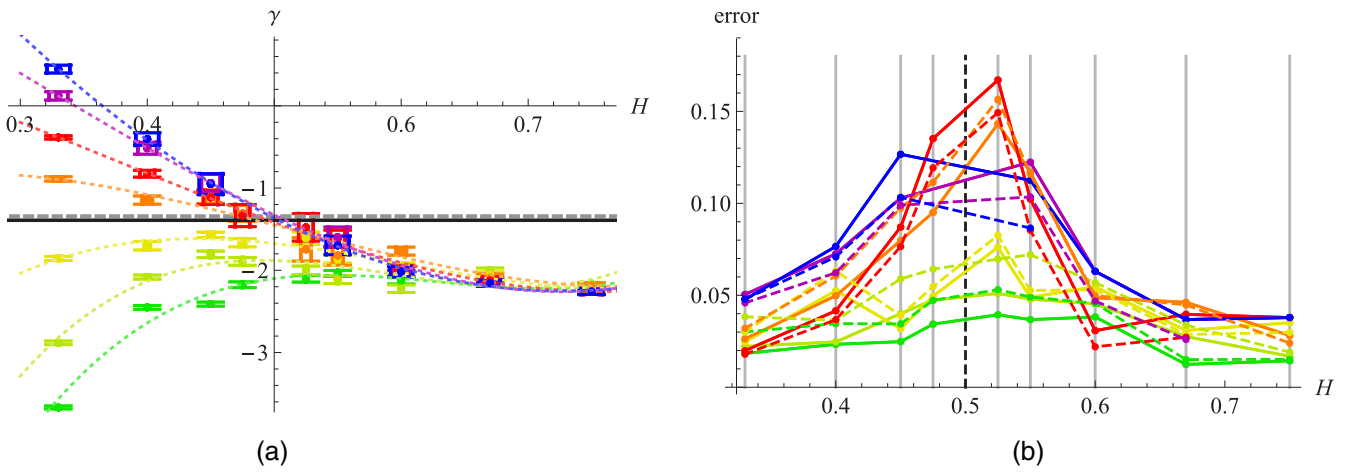

FIG. 3. Effective measured curvature γ, as a function of H and system size. The gray dashed line is γ as given by Eq. (118); the black solid line at -1.39 is a fit to the curvature of $\mathcal{F}(x)$ in the range 0.15–0.85. The color code is [from bottom to top in (a)] $N = 2^{13}$ (dark green), 2^{14} (green), 2^{16} (olive), 2^{18} (orange), 2^{20} (red), 2^{22} (dark magenta), and 2^{24} (blue). The 1-σ errors are indicated with bars in (a) and are explicitly shown in (b). There the solid lines are the measured errors obtained as follows: γ is estimated by fitting a parabola to each of the data sets presented in Fig. 12 and measuring the variance of the data minus the fit, which allows one to estimate the error of the fit, after calibration on white noise. The dashed lines are proportional to the square root of the number of samples, divided by $|\epsilon|$, and calibrated against the estimated data to have a second independent estimate. The gray lines are a guide to the eye, at the location of the H values considered, $H = 0.33$, 0.4, 0.45, 0.475, 0.525, 0.55, 0.6, 0.67, and 0.75.

Using the Poisson summation formula, an alternative form for $\mathbb{P}(z,t)$ is

$$\mathbb{P}(z,t) = \frac{1}{2} + \sum_{m=1}^{\infty} e^{-m^2\pi^2 t} \cos(m\pi z). \tag{16}$$

It is useful to consider its Laplace-transformed version. We define the Laplace transform of a function $F(t)$, with $t \geqslant 0$, and marked with a tilde as

$$\tilde{F}(s) := \int_0^{\infty} dt\, e^{-st} F(t). \tag{17}$$

This yields

$$\tilde{P}_+(x,y,s) = \frac{e^{-\sqrt{s}|x-y|} - e^{-\sqrt{s}(x+y)}}{2\sqrt{s}} - \frac{[\coth(\sqrt{s}) - 1]\sinh(\sqrt{s}x)\sinh(\sqrt{s}y)}{\sqrt{s}}. \tag{18}$$

According to Eq. (15), a form which only depends on $x - y$ and $x + y$ also exists. We use the form (18), since the factorization of the second term facilitates its integration.

B. Boundary currents and conservation of probability

Conservation of probability reads (the variable x is the initial condition, here a dummy variable)

$$\partial_t P_+(x,y,t) + \partial_y J(x,y,t) = 0. \tag{19}$$

Here J is the current, which from Eq. (19) can be identified as

$$J(x,y,t) = -\partial_y P_+(x,y,t). \tag{20}$$

Due to the Dirichlet conditions at $y = 0$ and $y = 1$, we have

$$\int_0^1 dy\, \partial_t P_+(x,y,t) = J(x,0,t) - J(x,1,t). \tag{21}$$

We find

$$J(x,y,t) = \frac{\pi}{4}\vartheta_3'\left(\frac{\pi}{2}(x-y), e^{-\pi^2 t}\right) + \frac{\pi}{4}\vartheta_3'\left(\frac{\pi}{2}(x+y), e^{-\pi^2 t}\right). \tag{22}$$

The derivatives of the elliptic ϑ functions are with respect to its first argument. The probability to exit at time t, when starting at x for time 0, reads

$$P_{\text{exit}}(x,t) = -J_{\text{tot}}(x,t) = J(x,1,t) - J(x,0,t) = \frac{\pi}{2}\left[\vartheta_3'\left(\frac{\pi}{2}(x-1), e^{-\pi^2 t}\right) - \vartheta_3'\left(\frac{\pi x}{2}, e^{-\pi^2 t}\right)\right]. \tag{23}$$

Going to Laplace variables, we find

$$-1 + s\int_0^1 dy\, \tilde{P}(x,y,s) = \tilde{J}(x,0,s) - \tilde{J}(x,1,s). \tag{24}$$

The outgoing currents of the Laplace transform are

$$-\tilde{J}(x,0,s) = \frac{\sinh(\sqrt{s}(1-x))}{\sinh(\sqrt{s})}, \tag{25}$$

$$\tilde{J}(x,1,s) = \frac{\sinh(\sqrt{s}\,x)}{\sinh(\sqrt{s})}. \tag{26}$$

C. Absorption probabilities at $x = 0$ and $x = 1$

The absorption probabilities at $x = 0$ and $x = 1$ are

$$P_0(x) := \int_0^{\infty} dt[-J(x,0,t)] = \lim_{s\to 0}[-\tilde{J}(x,0,s)] = 1 - x,$$
$$P_1(x) := \int_0^{\infty} dt\, J(x,1,t) = \lim_{s\to 0}\tilde{J}(x,1,s) = x. \tag{27}$$

D. Moments of the absorption time, starting at x

Moments of the absorption time are extracted from the Laplace-transformed currents as

$$\langle T_{\text{exit}}(x)\rangle_0 = -\partial_s[\tilde{J}(x,1,s) - \tilde{J}(x,0,s)]|_{s=0} = \frac{1}{2}x(1-x), \tag{28}$$

$$\int_0^1 dx \langle T_{\text{exit}}(x)\rangle_0 = \frac{1}{12}, \tag{29}$$

$$\begin{aligned}\langle T_{\text{exit}}(x)^2\rangle_0 &= \partial_s^2[\tilde{J}(x,1,s) - \tilde{J}(x,0,s)]|_{s=0} \\ &= \frac{1}{12}x(1-x)(1+x-x^2),\end{aligned} \tag{30}$$

$$\int_0^1 dx \langle T_{\text{exit}}(x)^2\rangle_0 = \frac{1}{60}. \tag{31}$$

E. Probabilities for the span

The numerical simulations we will perform later can be stopped when the *width* or *span* of the process reaches 1. The span is a classical problem treated, e.g., in [39–42], but the observable in question seems not to have been considered. Here we give an analytical result and validate it numerically. The two series expansions we obtain provide simple approximate solutions for both small and large times.

To properly define the problem, we note the positive and negative records (also known as the running maximum and minimum) as

$$M_+(t) := \max_{t' \leqslant t} X_{t'}, \tag{32}$$

$$M_-(t) := \min_{t' \leqslant t} X_{t'}. \tag{33}$$

The span $s(t)$ is their difference, i.e., the size of the (compact) domain visited up to time t,

$$s(t) := M_+(t) - M_-(t). \tag{34}$$

We want to know the probability that $s(t)$ becomes 1 for the first time. We denote this time by T_1 and its probability distribution by $P_{T_1}(t)$. It can be obtained as follows: The outgoing current at the lower boundary positioned at m_1, with the upper boundary at m_2, and starting at x is

$$\begin{aligned}&\mathbf{J}(x, m_1, m_2, t) \\ &= \frac{1}{(m_1-m_2)^2} J\left(\frac{x-m_1}{m_2-m_1}, 0, \frac{t}{(m_2-m_1)^2}\right).\end{aligned} \tag{35}$$

(The scale factor can be understood from the observation that the current is a density at the starting point times a spatial derivative of a probability.) The probability that the walk reaches m_2 before being absorbed at m_1 is $\partial_{m_2}\mathbf{J}(x, m_1, m_2, t)$. Finally, the probability to have span 1 at time t is this expression, integrated over x between the two boundaries, times a factor of 2. The latter accounts for the term where the two boundaries are exchanged. Setting, without loss of generality, $m_1 = 0$ and $m_2 = m$, this is written as

$$\begin{aligned}P_{T_1}(t) &= -2\partial_m \frac{1}{m^2}\int_0^m dx\, J\left(\frac{x}{m}, 0, \frac{t}{m^2}\right)\Big|_{m=1} \\ &= -2\partial_m \frac{1}{m}\int_0^1 dx\, J\left(x, 0, \frac{t}{m^2}\right)\Big|_{m=1} \\ &= 2(1+2t\partial_t)\int_0^1 dx\, J(x,0,t).\end{aligned} \tag{36}$$

Using Eqs. (20) and (15) allows us to rewrite the integral as

$$\begin{aligned}\int_0^1 dx\, J(x,0,t) &= \int_0^1 dx\, \partial_y[\mathbb{P}(x-y,t) - \mathbb{P}(x+y,t)]|_{y=0} \\ &= -2\int_0^1 dx\, \partial_x \mathbb{P}(x,t) \\ &= 2[\mathbb{P}(1,t) - \mathbb{P}(0,t)].\end{aligned} \tag{37}$$

Thus

$$P_{T_1}(t) = 4(1+2t\partial_t)[\mathbb{P}(1,t) - \mathbb{P}(0,t)]. \tag{38}$$

Inserting the definition (14) of $\mathbb{P}$, we get

$$\begin{aligned}P_{T_1}(t) &= 4(1+2t\partial_t)\sum_{n=-\infty}^{\infty}\frac{e^{-(2n+1)^2/4t} - e^{-n^2/t}}{\sqrt{4\pi t}} \\ &= \frac{1}{\sqrt{\pi}t^{3/2}}\sum_{n=-\infty}^{\infty}(2n+1)^2 e^{-(2n+1)^2/4t} - 4n^2 e^{-n^2/t} \\ &= 4\sqrt{\frac{t}{\pi}}\partial_t[\vartheta_2(0, e^{-1/t}) - \vartheta_3(0, e^{-1/t})].\end{aligned} \tag{39}$$

With the help of the Poisson-formula transformed Eq. (16), this can compactly be written as

$$P_{T_1}(t) = 8\sum_{n=0}^{\infty} e^{-\pi^2(2n+1)^2 t}[2\pi^2(2n+1)^2 t - 1]. \tag{40}$$

This result is compared to a numerical simulation in Fig. 4. Our expansions allow us to give simple formulas for the small- and large-t asymptotics,

$$P_{T_1}(t) \simeq \frac{2e^{-1/4t}}{\sqrt{\pi}t^{3/2}} + O(e^{-1/t}), \tag{41}$$

$$P_{T_1}(t) \simeq e^{-\pi^2 t}[16\pi^2 t - 8 + O(e^{-8\pi^2 t})]. \tag{42}$$

These expansions work in a rather large and overlapping domain, as can be seen in Fig. 4. Its Laplace transform is

$$\begin{aligned}\tilde{P}_{T_1}(s) &= 2(1+2s\partial_s)\sum_{n=-\infty}^{\infty}\int_0^{\infty} dt\, \frac{e^{-n^2/t} - e^{-(2n+1)^2/4t}}{\sqrt{\pi t}} e^{-st} \\ &= \frac{1}{\cosh(\sqrt{s}/2)^2}.\end{aligned} \tag{43}$$

Extracting the moments from the Laplace transform yields

$$\langle T_1\rangle = \tfrac{1}{4}, \quad \langle T_1^2\rangle = \tfrac{1}{12}, \quad \langle T_1^3\rangle = \tfrac{17}{480}, \ldots. \tag{44}$$

Finally, let us connect to the classical work on the span [39–42]. We will show how to reproduce formulas (3.7) and

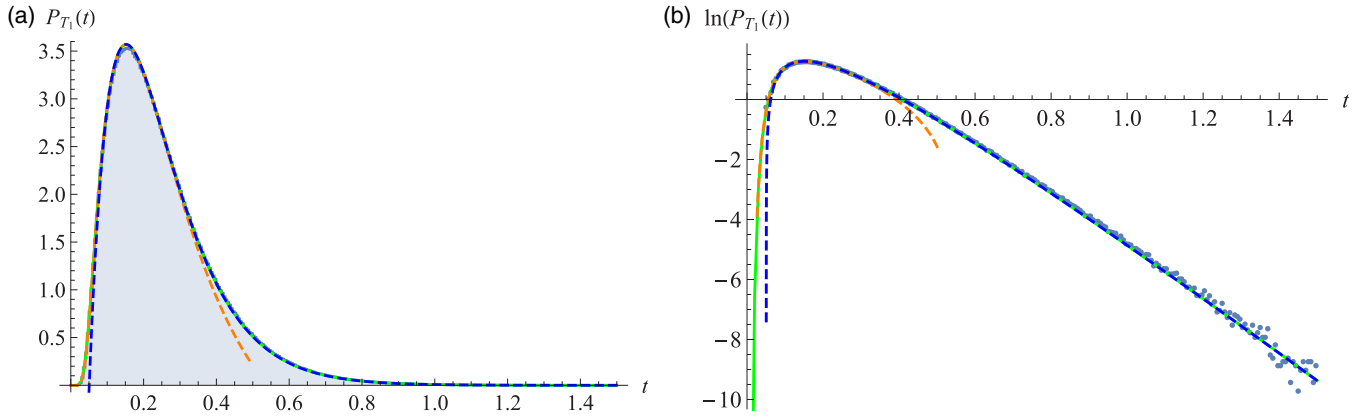

FIG. 4. (a) Probability that the span reaches 1 for the first time. Gray shading indicates the random-walk (RW) simulation with $\delta t = 10^{-5}$ and 10^6 samples, the green curve the analytic result (39), the orange dashed curve the small-time asymptote (41), and the blue dashed curve the large-time asymptote (42). Note a small systematic deviation due to the relatively large time step $\delta t = 10^{-5}$. (b) Same as (a) on a logarithmic scale.

(3.8) in [40]. The latter give the density $\rho_t(s)$ for the span s at time t. In our formalism, it can be obtained as

$$\rho_t(m_2 - m_1) = -\partial_{m_1}\partial_{m_2}\int_{m_1}^{m_2} dx \int_{m_1}^{m_2} dy\, \mathbf{P}(x, y, m_1, m_2, t), \tag{45}$$

where $\mathbf{P}(x, y, m_1, m_2, t)$ is the probability to go from x to y in time t, without being absorbed by the lower boundary positioned at m_1 or the upper boundary positioned at m_2. In terms of the propagator $P_+(x, y, t)$, this can be written as

$$\rho_t(s) = \partial_s^2\left[s\int_0^1 dx \int_0^1 dy\, P_+(x, y, t/s^2)\right]. \tag{46}$$

Using Eq. (15) and the series expansions (14) and (16) yields, after integration and simplifications, two different representations

$$\begin{aligned}\rho_t(s) &= \frac{4}{\sqrt{\pi t}}\sum_{n=1}^{\infty}(-1)^{n+1}n^2 e^{-n^2 s^2/4t} \\ &= \frac{16t}{s^5}\sum_{n=0}^{\infty} e^{-\pi^2(2n+1)^2 t/s^2}[2\pi^2(2n+1)^2 t - s^2]. \end{aligned}\tag{47}$$

This is equivalent to Eqs. (3.7) and (3.8) in [40], if there one replaces $t \to 2t$. [Our covariance (2) at $H = 1/2$ is $2t$ instead of t as in [40].] The small- and large-s asymptotics are

$$\rho_t(s) \simeq \frac{4}{\sqrt{\pi t}}[e^{-s^2/4t} - 4e^{-s^2/t} + O(e^{-9s^2/4t})], \tag{48}$$

$$\rho_t(s) \simeq \frac{16t}{s^5}e^{-\pi^2 t/s^2}[2\pi^2 t - s^2] + O(e^{-9\pi^2 t/s^2}). \tag{49}$$

Note that in Eq. (48) we have also retained the subleading term for small s, which considerably improves the numerical accuracy. A test is presented in Fig. 5.

III. CORRECTIONS TO THE ACTION FOR FBM

Here we briefly review the derivation of the effective action for FBM [30,31,34,36]. The exact action for a Gaussian process with correlations $\mathcal{C}(t_1, t_2)$ is, by definition,

$$\mathcal{S}[X] = \int_{0<t_1<t_2<T} \dot{X}_{t_1}\mathcal{C}^{-1}(t_1, t_2)\dot{X}_{t_2}. \tag{50}$$

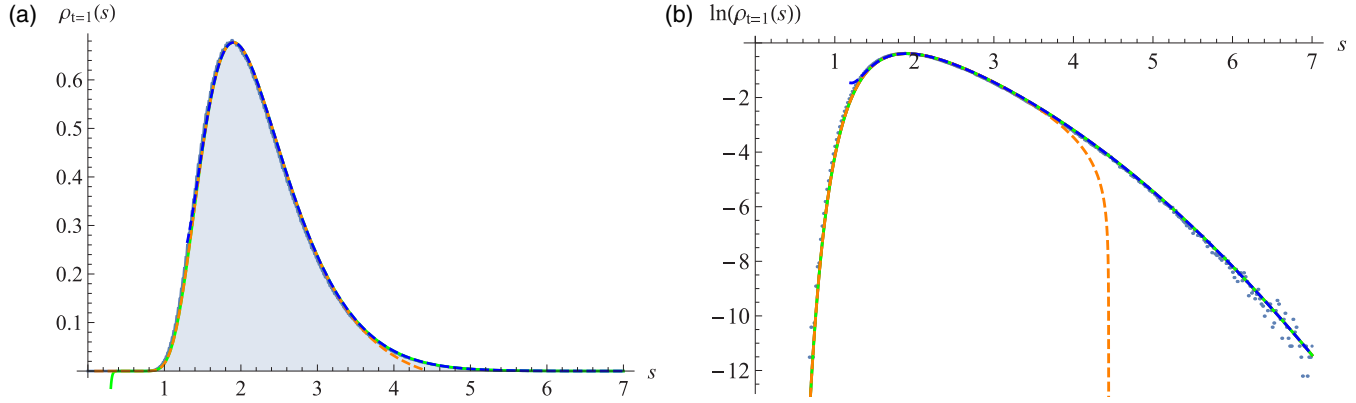

FIG. 5. (a) Density of the span at time $t = 1$. Gray shading indicates the RW simulation with $\delta t = 10^{-4}$ and 10^6 samples, the green curve the analytic result (47), the orange dashed curve the small-s asymptotics (48), and the blue dashed curve the large-s asymptotics (49). (b) Same as (a) but on a logarithmic scale.

Here

$$\begin{aligned}\mathcal{C}(t_1,t_2) &= \langle \dot{X}_{t_1}\dot{X}_{t_2}\rangle \\ &= 2\delta(t_1-t_2)2H|t_2-t_1|^{2H-1} \\ &\quad + 2H(2H-1)|t_1-t_2|^{2(H-1)} \\ &= 2D_\epsilon\left[\delta(t_1-t_2)+\frac{\epsilon}{|t_1-t_2|}+O(\epsilon^2)\right]. \end{aligned} \tag{51}$$

The diffusion constant, which depends on the small-time cutoff τ implicit in the above construction, reads

$$D_\epsilon \equiv 2H\tau^{2H-1} = (1+2\epsilon)\tau^{2\epsilon}. \tag{52}$$

This scale can be understood as follows: Our procedure yields a random process X_t, which is a Brownian process at times smaller than τ and a FBM at larger times.

The functional inverse of Eq. (51) which enters into the effective action (50) reads

$$\mathcal{C}^{-1}(t_1,t_2) = \frac{1}{2D_\epsilon}\left[\delta(t_1-t_2)-\frac{\epsilon}{|t_1-t_2|}+O(\epsilon^2)\right]. \tag{53}$$

This allows us to write the action (50) as the action of Brownian motion, plus a nonlocal term

$$S[X] = \mathcal{S}_0 + \epsilon\mathcal{S}_1 + O(\epsilon^2), \tag{54}$$

with

$$\mathcal{S}_0 := \frac{1}{4D_\epsilon}\int_t \dot{X}_t^2, \tag{55}$$

$$\mathcal{S}_1 := \int_{t_1<t_2} \delta\mathcal{C}^{-1}(t_1,t_2)\dot{X}_{t_1}\dot{X}_{t_2}. \tag{56}$$

Here $\delta\mathcal{C}^{-1}(t_1,t_2)$ is the nonlocal part ($t_1\neq t_2$) of $\mathcal{C}^{-1}(t_1,t_2)$ defined in Eq. (53).

We will use the trick to represent the propagator as $|t|^{-1} = \int_{y>0} e^{-y|t|}$, which allows us to treat a small-time cutoff τ for a momentum cutoff Λ. The relation between these two cutoffs can be inferred from

$$\begin{aligned}\int_0^T dt\int_0^\Lambda e^{-yt}dy &= \ln(T\Lambda)+\gamma_{\rm E}+O(e^{-T\Lambda}) \\ &\overset{!}{=} \ln(T/\tau) = \int_\tau^T \frac{dt}{t}. \end{aligned} \tag{57}$$

This implies that up to exponentially small terms

$$\Lambda = \frac{e^{-\gamma_{\rm E}}}{\tau}. \tag{58}$$

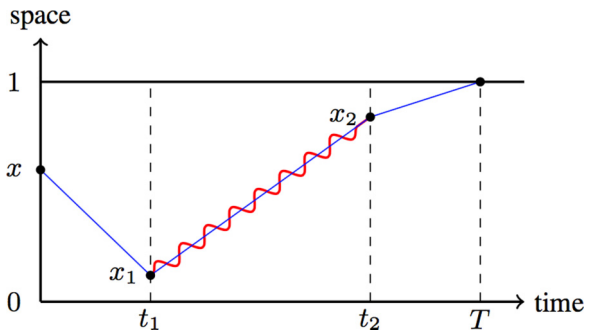

FIG. 6. Graphic representation of the path integral for the order-ϵ contribution $\tilde{A}(x,s)$ given in Eq. (60).

IV. ABSORPTION CURRENT AT ONE-LOOP ORDER

A. General formulas

We want to calculate the current at the upper boundary at time t, when starting at x at time 0. We denote this by calligraphic $\mathcal{J}(x,1,t)$, to distinguish it from the Brownian result $J(x,1,t)$. We follow the procedure outlined in Ref. [34], which works on the Laplace-transformed version. The outgoing current at order ϵ reads

$$\tilde{\mathcal{J}}(x,1,s) = \tilde{J}\left(x,1,\frac{s}{D_\epsilon}\right)+2\epsilon\tilde{A}(x,s)+O(\epsilon^2) = \tilde{J}(x,1,s)+2\epsilon[\tilde{A}(x,s)-(1+\ln\tau)s\partial_s\tilde{J}(x,1,s)]+O(\epsilon^2). \tag{59}$$

(The relation for the currents in time has an additional factor of $1/D_\epsilon$.) The first-order correction for the current at $y=1$ is

$$\tilde{A}(x,s) = \int_0^\Lambda dy\int_0^1 dx_1\int_0^1 dx_2\tilde{P}_+(x,x_1,s)\partial_{x_1}\tilde{P}_+(x_1,x_2,s+y)\,\partial_{x_2}\tilde{J}(x_2,1,s) \tag{60}$$

(see Fig. 6). The resulting expression after integration over x_1 and x_2 is rather lengthy, but can be simplified to

$$\begin{aligned}\tilde{A}(x,s) = \int_0^\Lambda dy\,\frac{\sqrt{s}}{2y^2\sinh(\sqrt{s+y})\sinh(\sqrt{s})}\Bigg[&\frac{\sinh(\sqrt{s}x)}{\sinh(\sqrt{s})}\{\sqrt{s+y}[3-4\cosh(\sqrt{s})\cosh(\sqrt{s+y})+\cosh(2\sqrt{s})] \\ &+y\cosh(\sqrt{s})\sinh(\sqrt{s+y})\}-\cosh(\sqrt{s}x)\{xy\sinh(\sqrt{s+y})+2\sqrt{s+y}[\cosh(\sqrt{s})-\cosh(\sqrt{s+y})]\} \\ &-2\sqrt{s+y}\cosh((1-x)\sqrt{s+y})+2\sqrt{s+y}\cosh(\sqrt{s})\cosh(x\sqrt{s+y})\Bigg]. \end{aligned} \tag{61}$$

As the integrand vanishes at $x=0$ and $x=1$,

$$\tilde{A}(0,s) = \tilde{A}(1,s) = 0. \tag{62}$$

The integral (61) is difficult to integrate analytically, or numerically. We will therefore study moments of s, which allow us to access the exit probability, and the first moments of the exit times. We start with the lowest moment, the exit probability.

B. Absorption probability at the upper boundary

The limit of $s \to 0$ in the integral (61) yields the correction to the probability to exit at the upper boundary, starting at x. Simplifying Eq. (61), we find

$$\tilde{A}(x,0) = \int_0^\infty dy \, \frac{e^{-x\sqrt{y}}(-2xe^{x\sqrt{y}+\sqrt{y}} + 2xe^{x\sqrt{y}} + e^{x\sqrt{y}+\sqrt{y}} - e^{x\sqrt{y}} + e^{2x\sqrt{y}} - e^{\sqrt{y}})}{(e^{\sqrt{y}}+1)y^{3/2}}. \tag{63}$$

We set the cutoff $\Lambda \to \infty$, as the integral is convergent. The current at the lower boundary is by symmetry

$$\tilde{A}(x,0) = -\tilde{A}(1-x,0). \tag{64}$$

To simplify this expression, we perform two variable transformations. The first sets $y = z^2$ and the second $z = -\ln(r)$. This yields

$$\tilde{A}(x,0) = -2\int_0^1 dr \, \frac{-r^{1-x} + r^x - 2rx + r + 2x - 1}{r(r+1)\ln^2(r)}. \tag{65}$$

This expression is still difficult to integrate, due to the logarithms in the denominator. Taking two derivatives simplifies this to

$$\partial_x^2 \tilde{A}(x,0) = 2\int_0^1 dr \, \frac{r^{-x} - r^{x-1}}{r+1} = -\frac{2}{x} - \psi\left(\frac{1}{2} - \frac{x}{2}\right) + \psi\left(1 - \frac{x}{2}\right) - \psi\left(\frac{x}{2} + \frac{1}{2}\right) + \psi\left(\frac{x}{2} + 1\right). \tag{66}$$

We now have to integrate twice with respect to x, which gives the result plus terms of the form $a + bx$. The latter can be fixed by Eq. (62). The result is

$$\tilde{A}(x,0) = \frac{1}{3}(2x-1)[\ln(2) - 3 + 36\zeta'(-1)] - 4\psi^{(-2)}\left(\frac{1}{2} - \frac{x}{2}\right) + 4\psi^{(-2)}\left(1 - \frac{x}{2}\right) + 4\psi^{(-2)}\left(\frac{x}{2}\right) - 4\psi^{(-2)}\left(\frac{x+1}{2}\right). \tag{67}$$

For $P_1'(x)$, we also need its first derivative

$$\partial_x \tilde{A}(x,0) = 2\left[12\zeta'(-1) + \frac{\ln(2)}{3} + \ln\left(\Gamma\left(\frac{1}{2} - \frac{x}{2}\right)\right) - \ln\left(\Gamma\left(1 - \frac{x}{2}\right)\right) + \ln\left(\Gamma\left(\frac{x}{2}\right)\right) - \ln\left(\Gamma\left(\frac{x+1}{2}\right)\right)\right]. \tag{68}$$

The Taylor expansion of $\tilde{A}(x,0)$ is

$$\tilde{A}(x,0) = x\left\{-2\ln(x) + \frac{8}{3}[9\zeta'(-1) + \ln(2)]\right\} + x^2\ln(4) + \frac{x^4\zeta(3)}{4} + \frac{x^6\zeta(5)}{8} + \frac{9x^8\zeta(7)}{128} + \frac{17x^{10}\zeta(9)}{384} + O(x^{12}). \tag{69}$$

Note the logarithmic term, which can be interpreted as a correction to the power law for $x \to 0$ in $P_1'(x)$. Indeed, scaling suggests [30,34,37]

$$\mathcal{P}'_{1,\text{scaling}}(x) = [x(1-x)]^{1/H-2}\frac{\Gamma\left(\frac{2}{H} - 2\right)}{\Gamma\left(\frac{1}{H} - 1\right)^2}. \tag{70}$$

The correction to Eq. (70) at order ϵ can be written as

$$\mathcal{P}'_1(x) = \mathcal{N}[x(1-x)]^{1/H-2}e^{\epsilon\mathcal{F}(x)}, \tag{71}$$

$$\begin{aligned}\mathcal{F}(x) &= 2\partial_x\tilde{A}(x,0) + 4\ln(x) + 4\ln(1-x) + 8 \\ &= 4\left[12\zeta'(-1) + \frac{\ln(2)}{3} + \ln(x(1-x)) + \ln\left(\Gamma\left(\frac{1}{2} - \frac{x}{2}\right)\right) - \ln\left(\Gamma\left(1 - \frac{x}{2}\right)\right) + \ln\left(\Gamma\left(\frac{x}{2}\right)\right) - \ln\left(\Gamma\left(\frac{x+1}{2}\right)\right)\right].\end{aligned} \tag{72}$$

We have chosen conventions such that $\int_0^1 dx\,\mathcal{F}(x) = 0$, moving the constant term into the normalization $\mathcal{N}$. The latter has to be chosen such that $\int_0^1 dx\,\mathcal{P}'_1(x) = 1$. The function $\mathcal{F}(x)$ is plotted in Fig. 2. It has a regular Taylor expansion around $x = 0$,

$$\mathcal{F}(x) = \tfrac{4}{3}[36\zeta'(-1) + 3 + 4\ln(2)] + x[\ln(256) - 4] - 2x^2 + \tfrac{2}{3}x^3[3\zeta(3) - 2] - x^4 + \tfrac{1}{10}x^5[15\zeta(5) - 8] + O(x^6). \tag{73}$$

For numerical purposes, a Taylor expansion around $x = 1/2$ is appropriate (with error < 0.002),

$$\begin{aligned}\mathcal{F}(x) &= 48\zeta'(-1) - 8\ln\Gamma\left(\tfrac{3}{4}\right) + 8\ln\Gamma\left(\tfrac{1}{4}\right) + 4 - \tfrac{20}{3}\ln(2) + 16(C-1)\left(x - \tfrac{1}{2}\right)^2 \\ &\quad + \tfrac{1}{48}\left(x - \tfrac{1}{2}\right)^4\left[\psi^{(3)}\left(\tfrac{1}{4}\right) - \psi^{(3)}\left(\tfrac{3}{4}\right) - 1536\right] + O\left(x - \tfrac{1}{2}\right)^6 \\ &= 0.116\,736 - 1.344\,55\left(x - \tfrac{1}{2}\right)^2 - 0.353\,774\left(x - \tfrac{1}{2}\right)^4 + O\left(x - \tfrac{1}{2}\right)^6.\end{aligned} \tag{74}$$

Validation of this function via a numerical simulation is given in Figs. 12 and 13.

C. Resummation

In Eq. (71) we had written the scaling function $\mathcal{F}(x)$ in the exponential. Since our calculation is performed at first order in ϵ, other forms are possible,

$$\mathcal{P}_1'(x) = \mathcal{N}[x(1-x)]^{1/H-2} e^{\epsilon \mathcal{F}(x)} + O(\epsilon^2) \quad (75)$$

$$= \mathcal{N}[x(1-x)]^{1/H-2}[1+\epsilon \mathcal{F}(x)] + O(\epsilon^2) \quad (76)$$

$$= \mathcal{N}[x(1-x)]^{1/H-2} \frac{1}{1-\epsilon \mathcal{F}(x)} + O(\epsilon^2). \quad (77)$$

The question arises which one to choose. There are many good reasons to choose the form (75).

(i) Adding drift μ to Brownian motion, the latter appears as an additive term in the exponential

$$P_+^{\mu}(x,y,t) = e^{\mu(y-x)/2-\mu^2 t/4} P_+(x,y,t). \quad (78)$$

(ii) The first-order correction (68) contains logarithmic terms, visible in Eq. (69). Having them in the exponential, they are resummed into power laws, according to

$$e^{\epsilon \ln(x)} = x^{\epsilon}. \quad (79)$$

This is how in Eq. (71) the scaling function of the Brownian, $x(1-x)$, was changed into $[x(1-x)]^{1/H-1}$. At the same time, the scaling function $\mathcal{F}(x)$, defined in Eq. (72), becomes regular for $x \to 0$, as can be seen in Eq. (73).

(iii) In field theory, perturbative corrections are in general, and most efficiently, calculated for the effective action, i.e., the logarithm of the partition function. In a thermodynamic setting as the one here, the effective action can be interpreted as the free energy.

(iv) Finally, as the exponential function is always positive for real arguments, the form (75) remains positive even when $\epsilon \mathcal{F}(x)$ becomes large. This is a necessary condition for a probability density.

For all these reasons, using the exponentiated version is the most natural choice, and the one chosen throughout this article. When corrections are large, which is especially important for universal amplitudes, we will compare this choice with the linear extrapolation (76).

D. Expectation of exit time

The nontrivial one-loop correction to $\langle T_{\text{exit}}(x)\rangle$ given in Eq. (28) is 2ϵ times

$$\mathcal{B}(x) := -\partial_s[\tilde{\mathcal{A}}(x,s) + \tilde{\mathcal{A}}(1-x,s)]|_{s=0}. \quad (80)$$

Note that this combination is much simpler than the unsymmetrized one, which will allow us to integrate it analytically. We find with the same variable transformations as above

$$\mathcal{B}(x) = \int_{e^{-\sqrt{\Lambda}}}^1 dr \left[\frac{1}{r\left(\frac{1}{r^{x-1}-1} + \frac{1}{1-r^x}\right)\ln^2(r)} + \frac{(1-x)x}{r\ln(r)} \right]. \quad (81)$$

Both terms can be integrated, the first after taking two derivatives with respect to x. Integrating twice with respect to x and fixing the lost terms of the form $a+bx$ by demanding, according to Eq. (62), that $\mathcal{B}(0) = \mathcal{B}(1) = 0$ yields[1]

$$\mathcal{B}(x) = [\gamma_{\text{E}}(x-1)+1]x - x\ln(x) + \tfrac{1}{2}(x-1)x\ln(\Lambda) + \psi^{(-2)}(1-x) + \psi^{(-2)}(x+1) - \ln(2\pi). \quad (82)$$

Taylor expanding for small $x(1-x)$, we find

$$\frac{2\epsilon\mathcal{B}(x)}{\langle T_{\text{exit}}(x)\rangle_0} = -4\epsilon[\gamma_{\text{E}} - 1 + \ln(x(1-x)\sqrt{\Lambda})] + O(x(1-x)). \quad (83)$$

This is consistent with

$$\langle T_{\text{exit}}(x)\rangle = \frac{1}{D_\epsilon}\langle T_{\text{exit}}(x)\rangle_0 + 2\epsilon\mathcal{B}(x) + O(\epsilon^2) \sim [x(1-x)]^{1/H-1} + O(\epsilon^2). \quad (84)$$

Let us define

$$\mathcal{F}_T(x) := \frac{2\mathcal{B}(x)}{\langle T_{\text{exit}}(x)\rangle_0} + 4[\ln(\sqrt{\Lambda}(1-x)x) + \gamma_{\text{E}} - 1]$$

$$= \frac{4}{x(1-x)}\{x^2 + x[(1-x)\ln(1-x) - x\ln(x)] + \psi^{(-2)}(1-x) + \psi^{(-2)}(x+1) - \ln(2\pi)\}. \quad (85)$$

This function is plotted in Fig. 7(a) (and numerically validated in Fig. 8 and more precisely in Fig. 14).

E. Expectation of exit time squared $\langle T_{\text{exit}}(x)^2\rangle$

The first-order correction to $\langle T_{\text{exit}}(x)^2\rangle$ given in Eq. (28) is 2ϵ times

$$\mathcal{C}(x) := \partial_s^2[\tilde{\mathcal{A}}(x,s) + \tilde{\mathcal{A}}(1-x,s)]|_{s=0}. \quad (86)$$

Again, this combination is much simpler than the unsymmetrized one. We find, with the same variable transformations as above,

$$\mathcal{C}(x) = \int_{e^{-\sqrt{\Lambda}}}^1 dr \left[\frac{1}{r\left(\frac{r}{r-r^x} + \frac{1}{r^x-1}\right)\ln^4(r)} + \frac{xr^{1-x} + xr^{x-1} - xr^{-x} + r^{-x} - xr^x + r^x - 2}{(r-1)^2\ln^3(r)} + \frac{r^{1-x} + r^x + (r+1)[6(x-1)x-1]}{6(r-1)r\ln^2(r)} + \frac{x^4 - 2x^3 + x}{3r\ln(r)} \right]. \quad (87)$$

Anticipating that a good approximation is given by $\langle T^2(x)\rangle \sim [\langle T_{\text{exit}}^2(x)\rangle_0]^{1/H-1}$, we set, with normalization $\mathcal{N}$,

$$\langle T_{\text{exit}}^2(x)\rangle = \mathcal{N}\left[\langle T_{\text{exit}}^2(x)\rangle_0\right]^{1/H-1} e^{\epsilon\mathcal{F}_{T^2}(x)+O(\epsilon^2)}. \quad (88)$$

[1] Note that there are corrections in the boundary region of the form $e^{-\sqrt{\Lambda}x}/x$. These might be interpreted as the finite-discretization corrections seen in the simulations of Sec. V. We did not try to make this statement quantitative.

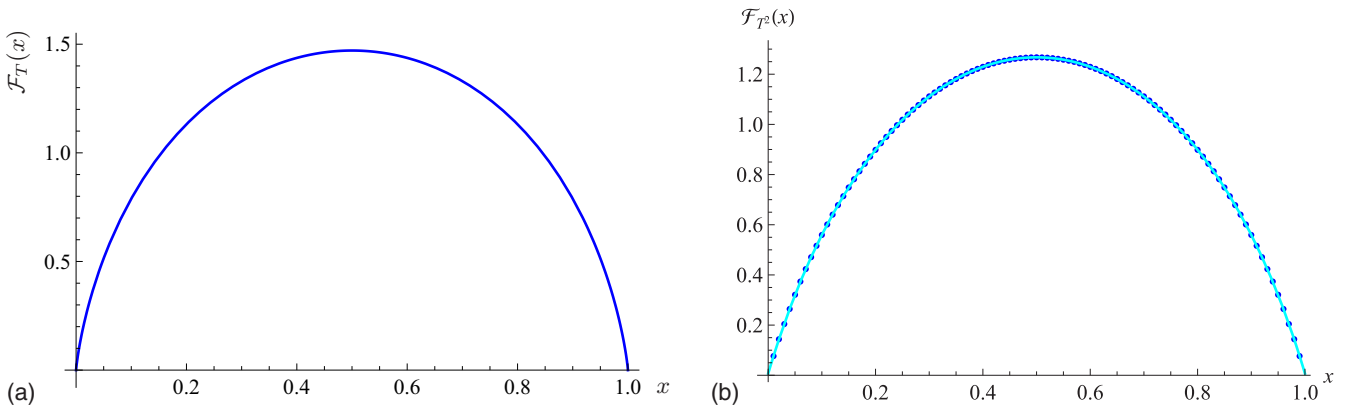

FIG. 7. (a) Function $\mathcal{F}_T(x)$, defined in Eq. (85). (b) Function $\mathcal{F}_{T^2}(x)$, defined in Eq. (89). The dots are the numerically obtained points and the line is the fit of Eq. (90).

This implies that up to a constant, which will notably depend on the UV cutoff Λ,

$$\mathcal{F}_{T^2}(x) = 2\mathcal{C}(X) + 4\ln\left(\left\langle T_{\rm exit}^2(x)\right\rangle_0\right) + \text{const}$$
$$= 2\mathcal{C}(X) + 4\ln(x(1-x)(1+x-x^2)) + \text{const}. \quad (89)$$

We did not succeed in integrating Eq. (87) analytically. A numerical integration can be done without difficulty and yields the points in Fig. 7(b). A fit with a symmetric polynomial of degree 8 (with a total systematic plus numerical deviation smaller than 10^{-3}) reads

$$\mathcal{F}_{T^2}(x) \approx 1.260\,33 - 3.733\,28\left(x-\tfrac{1}{2}\right)^2 - 4.166\,28\left(x-\tfrac{1}{2}\right)^4$$
$$+ 5.241\,29\left(x-\tfrac{1}{2}\right)^6 - 38.0198\left(x-\tfrac{1}{2}\right)^8. \quad (90)$$

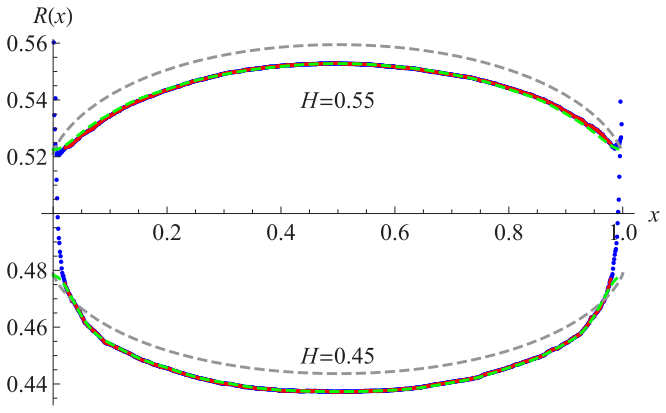

FIG. 8. Ratio $R(x)$ defined in Eq. (96). Shown in gray are the analytical (parameter-free) predictions and in red or blue are the data points of numerical simulations, presented in Sec. V. The red data points have been used to extract via a polynomial fit of order 40 (dashed green line) $R(0)$, with the result $R^{\rm num}_{H=0.45}(0) = 0.478$ and $R^{\rm num}_{H=0.55}(0) = 0.522$. Analytically, Eq. (97) yields $R^{\rm ana}_{H=0.45}(0) = 0.479$ and $R^{\rm ana}_{H=0.55}(0) = 0.521$. The deviation in the middle of the domain is of order 7×10^{-3}, consistent with an $O(\epsilon^2)$ correction to $R(x)$ of amplitude 3. More robust tests of our formulas, focusing on the shape of $R(x)$ and the spatially averaged exit times, are presented in Sec. V C.

Validation via a numerical simulation is presented in Fig. 14.

F. Estimation of timescales: Mean exit time

Up to now, we considered universal functions, without explicit evaluation of the proper timescales. This is motivated by the observation that timescales are often more sensitive to details of the implementation than amplitude ratios, such as those encoded in the functions $\mathcal{F}(x)$, $\mathcal{F}_T(x)$, and $\mathcal{F}_{T^2}(x)$. Nevertheless, our formalism is able to compute universal amplitudes, a task we turn to now.

We start by the simplest such observable, the mean exit time in the strip. By mean we understand an average over the starting position x and the realization of the process. According to Eqs. (28), (59), and (80),

$$\int_0^1 \langle T_{\rm exit}(x)\rangle dx$$
$$= -\partial_s|_{s=0}\int_0^1 dx\left[\tilde{J}\left(x,1,\frac{s}{D_\epsilon}\right) - \tilde{J}\left(x,0,\frac{s}{D_\epsilon}\right)\right]$$
$$+ 2\epsilon[\tilde{A}(x,s) - \tilde{A}(1-x,s)]$$
$$= \int_0^1 \frac{x(1-x)}{2D_\epsilon} + 2\epsilon\mathcal{B}(x)dx. \quad (91)$$

Recalling the definition of $\mathcal{F}_T(x)$ in Eq. (85), this can be rewritten as

$$\int_0^1 \langle T_{\rm exit}(x)\rangle dx$$
$$= \frac{1}{12D_\epsilon} + \frac{\epsilon}{2}\int_0^1 dx\,\mathcal{F}_T(x)x(1-x)$$
$$- 2\epsilon\int_0^1 x(1-x)[\ln(\sqrt{\Lambda}x(1-x)) + \gamma_{\rm E} - 1]dx. \quad (92)$$

The terms in question are

$$\frac{1}{2}\int_0^1 \mathcal{F}_T(x)x(1-x)\,dx = -\frac{5}{9} - 4\zeta'(-1)$$
$$= 0.106\,129\ldots \quad (93)$$

$$-2\int_0^1 x(1-x)[\ln(\sqrt{\Lambda}x(1-x))+\gamma_{\rm E}-1]dx$$
$$=-\frac{\ln(\Lambda)}{6}-\frac{\gamma_{\rm E}}{3}+\frac{8}{9}=0.696\,484\ldots-\frac{\ln(\Lambda)}{6}. \quad (94)$$

This yields

$$\int_0^1 \langle T_{\rm exit}(x)\rangle dx$$
$$=\frac{1}{12}\{1+2\epsilon[1-\gamma_{\rm E}-24\zeta'(-1)]+O(\epsilon^2)\}$$
$$=\frac{1}{12}[1+8.785\,78\epsilon+O(\epsilon^2)]$$
$$=\frac{1}{12}\exp(8.785\,78\epsilon)+O(\epsilon^2). \quad (95)$$

Note that all cutoff dependence has canceled, as expected. In the last two lines we gave two alternative resummations: the linear order-ϵ term and an exponential resummation, which was beneficial in resumming logarithms into a change in power law. We will see later (Fig. 15) that the numerically obtained result lies between the two expressions.

G. Exit times in the limit of $x \to 0$

Another interesting limit is $x \to 0$, also considered analytically in Ref. [43]. Let us define the ratio

$$R(x) := \frac{\langle T_{\rm exit}(x)\rangle}{[x(1-x)]^{1/H-1}}. \quad (96)$$

As in the preceding section, we derive, for $x \to 0$,

$$R(0) := \lim_{x\to 0} R(x) = \tfrac{1}{2}+\epsilon(1-\gamma_{\rm E})+O(\epsilon^2). \quad (97)$$

A test is given in Fig. 8. This limit agrees[2] with the equivalent object calculated in Ref. [43].

H. Time scales: Second moment of the exit time

Analogously to the derivation of Eq. (91), we have

$$\int_0^1 \langle T_{\rm exit}(x)^2\rangle dx$$
$$=\partial_s^2|_{s=0}\int_0^1 dx\left[\tilde{\jmath}\left(x,1,\frac{s}{D_\epsilon}\right)-\tilde{\jmath}\left(x,0,\frac{s}{D_\epsilon}\right)\right]$$
$$+2\epsilon[\tilde{A}(x,s)-\tilde{A}(1-x,s)]$$
$$=\int_0^1 \frac{x(1-x)(1+x-x^2)}{12D_\epsilon^2}+2\epsilon\mathcal{C}(x)dx. \quad (98)$$

The first integral is

$$\int_0^1 \frac{x(1-x)(1+x-x^2)}{12D_\epsilon^2}dx=\frac{1}{60D_\epsilon^2}. \quad (99)$$

The x integral over $\mathcal{C}(x)$ defined in Eq. (87) can be done analytically. The remaining nontrivial integral reads

$$\int_0^1 \mathcal{C}(x)dx=\int_{e^{-\sqrt{\Lambda}}}^1 dr\left[\frac{r+1}{3r(1-r)\ln^2(r)}+\frac{r+1}{(r-1)r\ln^4(r)}\right.$$
$$\left.+\frac{\frac{1}{3r}-\frac{2}{(r-1)^2}}{\ln^3(r)}+\frac{1}{15r\ln(r)}\right]. \quad (100)$$

This integral is hard to evaluate analytically. A precise numerical estimation can be obtained as follows: Taylor expand the integral at small r and integrate to show that

$$\int_0^1 \mathcal{C}(x)dx \simeq \text{const}+\frac{1}{3\Lambda^{3/2}}-\frac{1}{3\sqrt{\Lambda}}+\frac{1}{6\Lambda}-\frac{\ln(\Lambda)}{30}. \quad (101)$$

The integral (100) can then be integrated numerically. To this aim, one splits it into two pieces: the region close to $r=1$, for which one Taylor expands the integrand around $r=1$ and then integrates symbolically, and the remaining region, with cutoff Λ. Subtracting the terms in Eq. (101) from the numerically evaluated integral allows us to obtain the latter precisely already for relatively small Λ. The result of this procedure is

$$\int_0^1 \mathcal{C}(x)dx=0.152\,119-\frac{\ln(\Lambda)}{30}+O\left(\frac{1}{\sqrt{\Lambda}}\right). \quad (102)$$

This yields, for the second moment of the exit time,

$$\int_0^1 \langle T_{\rm exit}(x)^2\rangle dx=\frac{1}{60}[1+16.5632\epsilon+O(\epsilon^2)]$$
$$=\frac{1}{60}\exp(16.5632\epsilon+O(\epsilon^2)). \quad (103)$$

Note that all cutoff dependence has canceled, as it should. The result is compared with numerical simulations in Fig. 15(b).

I. Corrections to $\langle T_1\rangle$

In Eq. (36) we established that for Brownian motion

$$P_{T_1}(t)=2(1+2t\partial_t)\int_0^1 dx\,J(x,0,t)$$
$$=(1+2t\partial_t)\int_0^1 dx[J(x,0,t)-J(x,1,t)]. \quad (104)$$

The generalization to FBM at order ϵ is obtained as in the previous sections as

$$\mathcal{P}_{T_1}(t)=\left(1+\frac{t}{H}\partial_t\right)\int_0^1 dx[\mathcal{J}(x,0,t)-\mathcal{J}(x,1,t)]. \quad (105)$$

The factor of $1/H$ comes from the fact that the derivative in Eq. (36) was with respect to m and the scaling variable now is m/t^H. We conjecture that this result remains valid to all orders

[2]Using in the Supplemental Material of [43] $\psi(t)=2Dt^{2H}$ yields $\psi_0(t)=2Dt$ and $\psi_1(t)=4Dt\ln(t)$. Equation (G48) therein (generalized to arbitrary D) becomes $Tp_s(0)=\frac{x_0}{2D}+\epsilon\frac{x_0}{D}[1-\gamma_{\rm E}-2\ln(x_0)+4\ln(D)]+O(\epsilon^2)$. Setting $D=1$, we get $\lim_{x\to 0} Tp_s(0)/x^{1/H-1}=\frac{1}{2}+\epsilon(1-\gamma_{\rm E})$, which agrees with $R(0)$ in Eq. (97). The order-ϵ correction extracted from the simulation data of Ref. [43] is consistent with this value.

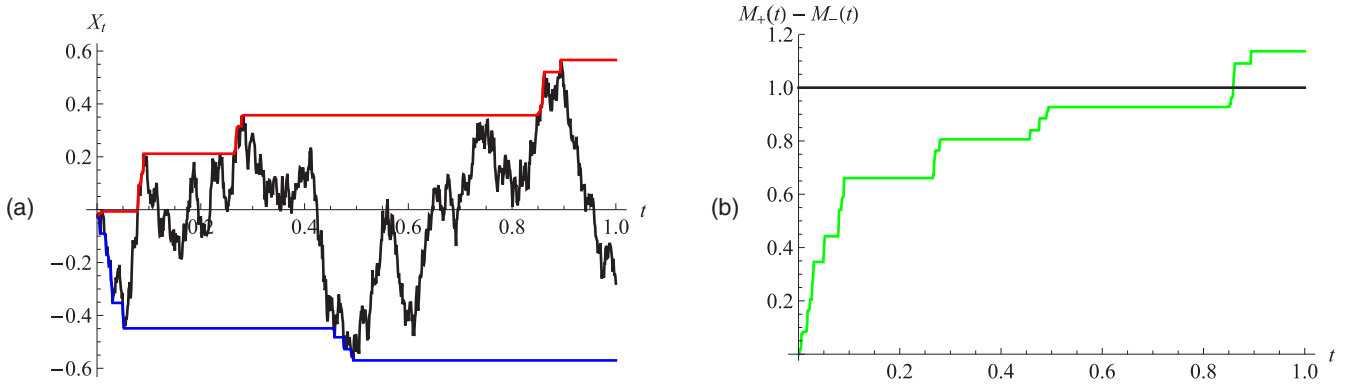

FIG. 9. (a) Random process X_t, with its running maximum (in red) and minimum (in blue) (see the text). (b) Span, i.e., running maximum minus running minimum.

in ϵ such that

$$\mathcal{P}_{T_1}(t) = \left(1 + \frac{t}{H}\partial_t\right) \int_0^1 dx\, \mathcal{P}_{\text{exit}}(x,t). \tag{106}$$

As a consequence,

$$\langle T_1^n \rangle = \left(1 + \frac{n}{H}\right) \int_0^1 dx \langle T_{\text{exit}}^n(x) \rangle. \tag{107}$$

For the first two moments, this yields

$$\begin{aligned} \langle T_1 \rangle &= \frac{1}{4} + \epsilon\left[\frac{1}{6} - 12\zeta'(-1) - \frac{\gamma_{\text{E}}}{2}\right] + O(\epsilon^2) \\ &= \frac{1}{4}[1 + 7.452\,45\epsilon + O(\epsilon^2)] \\ &= \frac{1}{4}\exp(7.452\,45\epsilon + O(\epsilon^2)), \end{aligned} \tag{108}$$

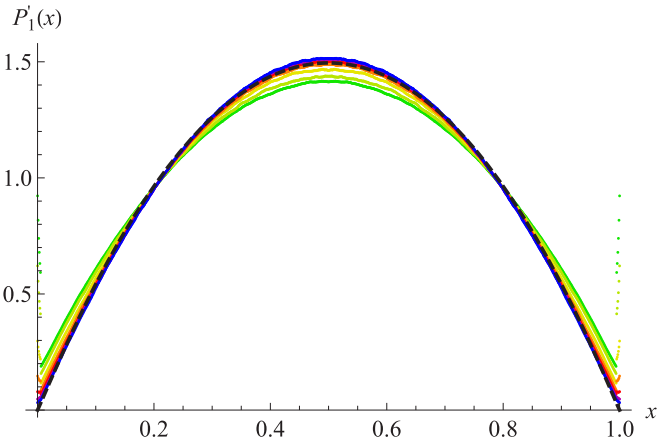

FIG. 10. Measured probability $P_1'(x)$ for $H = 0.33$. The system sizes are (from bottom to top at $x = 0.5$) $N = 2^{13}$ (dark green), 2^{14} (green), 2^{16} (olive), 2^{18} (orange), 2^{20} (red), 2^{22} (dark magenta), and 2^{24} (blue). The dashed line is the scaling ansatz (70) (i.e., almost a parabola). Note the slow convergence for $x \to 0$ and $x \to 1$. Also note that the measured result for the largest system size at $x = 1/2$ is larger than the scaling ansatz (70). This is equivalent to a positive curvature of the function $\mathcal{F}(x)$ defined in Eqs. (71) and (72) and given in Fig. 12(a).

$$\begin{aligned} \langle T_1^2 \rangle &= \frac{1}{12}[1 + 14.9632\epsilon + O(\epsilon^2)] \\ &= \frac{1}{12}\exp(14.9632\epsilon + O(\epsilon^2)). \end{aligned} \tag{109}$$

As usual, we have given two possible resummations. This will be tested later (see Fig. 16).

V. NUMERICAL VALIDATION

A. Algorithm

A numerical estimation of the calculated observables is obtained using the discrete-time algorithm by Davies and Harte [10], as described in [11,12]. It generates, for FBM of a given H sample, trajectories over a discretized time window [0,1]; the trajectories are drawn from a Gaussian probability with covariance (2). Time and space are then rescaled with respect to Eq. (2) such that no more than 10^{-4} of all samples fail to exit for a given H. (The timescales in question are the upper times in the plots of Fig. 17.) While this induces a small systematic error, we can take advantage of the lin-log

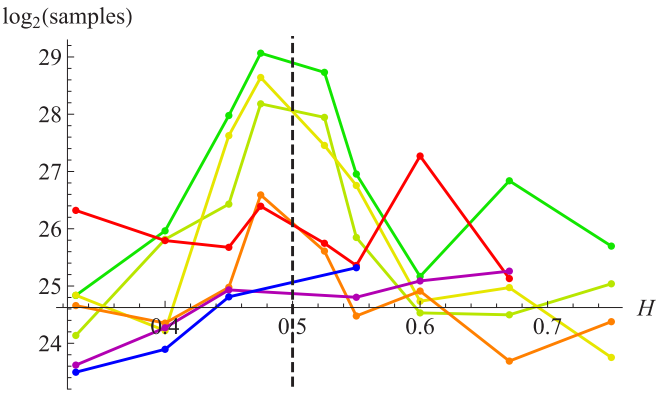

FIG. 11. Number of samples for each system size and value of H. The color code is as in Fig. 10. Since the measured signal is proportional to ϵ, the error scales like the square root of the number of samples divided by $|\epsilon|$. Thus more samples are needed for H close to $1/2$, and only small systems can be simulated for $H = 0.475$ and $H = 0.525$.

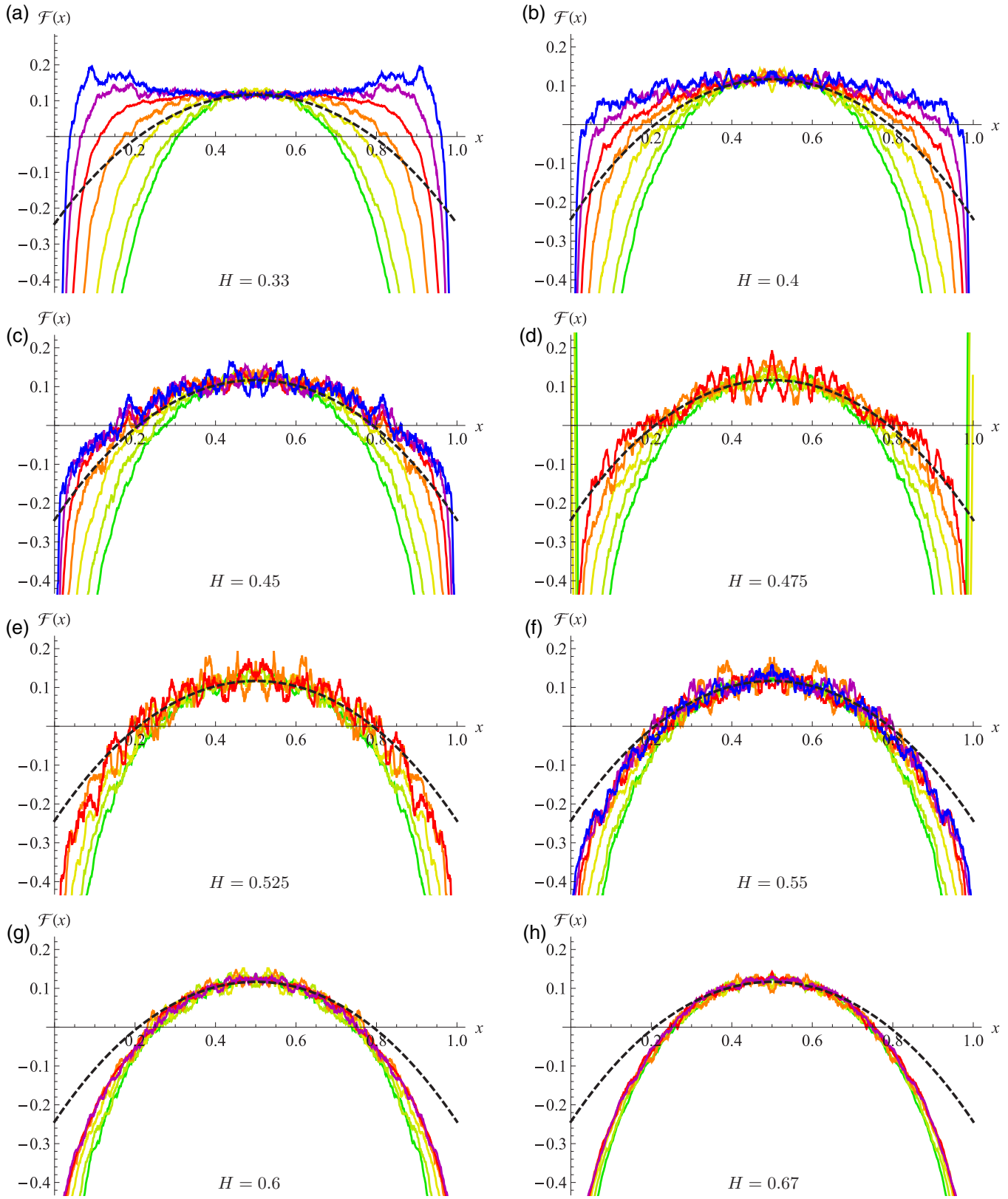

FIG. 12. (a)-(h) Numerically estimated scaling function $\mathcal{F}(x)$ for (from top to bottom) $N = 2^{13}$ (dark green), 2^{14} (green), 2^{16} (olive), 2^{18} (orange), 2^{20} (red), 2^{22} (dark magenta), and 2^{24} (blue). The black dashed line is the result of Eq. (72). For $\epsilon = \pm 0.025$, i.e., $H = 0.475$ and $H = 0.525$, due to the large statistics needed, we only simulated systems up to size $N = 2^{20}$. For $H \geqslant 0.6$, convergence in system size is good, and we skipped the largest system $N = 2^{24}$. Note that the scaling ansatz of (70), i.e., $\mathcal{P}'_{1,\text{scaling}}(x) \sim [x(1-x)]^{1/H-2}$ is equivalent to $\mathcal{F}(x) \equiv 0$.

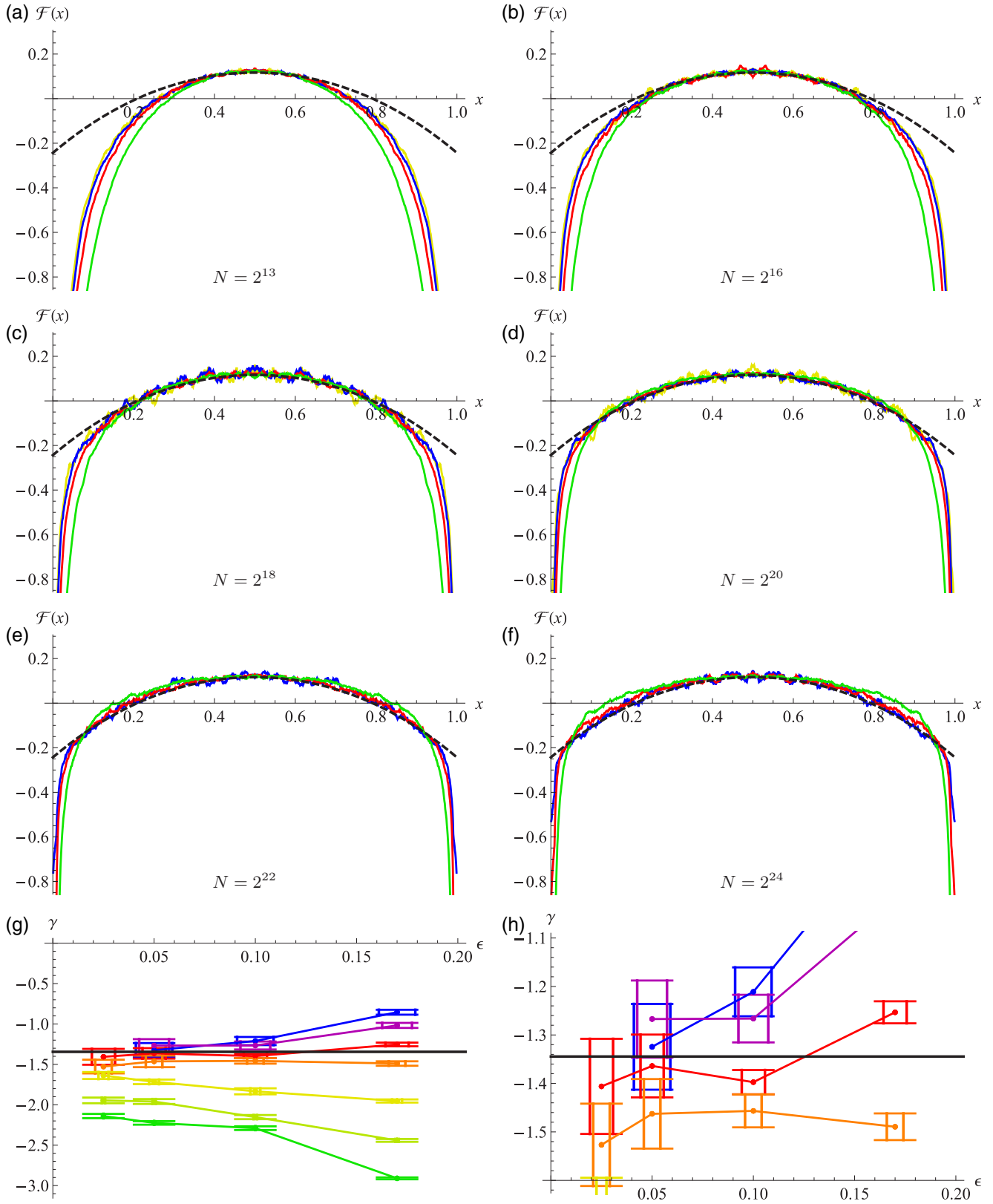

FIG. 13. (a)-(f) Dependence of the scaling function $\mathcal{F}(x)$ on N, by taking the mean between $H = 1/2 \pm \epsilon$, for $H = 0.33/0.67$ (green), $H = 0.4/0.6$ (red), $H = 0.45/0.55$ (blue), and $H = 0.475/0.525$ (olive and yellow). For $N = 2^{24}$, we have replaced the estimate for $H \geqslant 0.6$ by those of $N = 2^{22}$, justified by the much better convergence in system size for these values of H (see Fig. 12). Shown in (g) and (h) is the extracted curvature γ with system sizes increasing from bottom to top: $N = 2^{13}$ (green), $N = 2^{14}$ (bright green), $N = 2^{16}$ (olive and yellow), $N = 2^{18}$ (orange), $N = 2^{20}$ (red), $N = 2^{22}$ (violet), and $N = 2^{24}$ (blue, single dot with big error bars). For the error estimate see Fig. 3. Note that the scaling ansatz of (70), i.e., $\mathcal{P}'_{1,\text{scaling}}(x) \sim [x(1-x)]^{1/H-2}$, is equivalent to $\mathcal{F}(x) \equiv 0$.

performance of the Davies-Harte algorithm [10–12], whereas the execution time for a sequential generation of the sequence grows quadratically in time. Given the necessary system size, this would be very inefficient.

B. Exit probability

In order to measure $P_1(x)$ one could start the process X_t at x and measure whether X_t is first absorbed at $x = 0$ or $x = 1$. This is very inefficient, as for each x one has to run a simulation and repeat the latter until the statistics is good enough. A slightly better strategy is to start with $X_0 = 0$, generate X_t, shift it by x, and check for each x, whether it is first absorbed at $x = 0$ or $x = 1$. There is however a much more clever procedure, which we explain now and which is illustrated in Fig. 9. Define, for a random process X_t, the running maximum and minimum

$$M_+(t) := \max_{0<t'<t} X_{t'}, \tag{110}$$

$$M_-(t) := \min_{0<t'<t} X_{t'}. \tag{111}$$

The total width or span $s(t) := M_+(t) - M_-(t)$ grows monotonically. We are interested in the time T_1 when it attains 1. Define

$$T_1 := \min_t(M_+(t) - M_-(t) \geqslant 1), \tag{112}$$

$$x_0 := X_{T_1} \equiv \frac{X_{T_1}}{M_+(T_1) - M_-(T_1)}. \tag{113}$$

If the process starts for $x > x_0$, it will first be absorbed by the upper boundary (at $x = 1$), whereas if it starts for $x < x_0$, it will first be absorbed by the lower one (at $x = 0$). Denote the probability distribution of x_0 by $P_{x_0}(x)$. It satisfies

$$P_{x_0}(x) = -P_0'(x) = P_1'(x). \tag{114}$$

An example of the measurement of $P_1'(x)$ for $H = 0.33$ is shown in Fig. 10 (see also Fig. 11). The most remarkable feature of this plot is the very slow convergence in system size towards the asymptotic curve, which via scaling is very close to a parabola [see Eqs. (70) and (71)]. This slow convergence can also be seen on the distribution $P_{T_1}(t)$ of the times T_1 defined in Eq. (112). This is plotted in Fig. 17.

The slow convergence of $P_1'(x)$ can better be seen via the function $\mathcal{F}(x)$: An estimate of the latter can be extracted from the simulations, by inverting Eq. (71),

$$\mathcal{F}^\epsilon_{\text{num}}(x) := \frac{1}{\epsilon}\ln(P'(x)[x(1-x)]^{2-1/H}) + \text{const.} \tag{115}$$

The constant is chosen such that $\mathcal{F}^\epsilon_{\text{num}}(1/2) = \mathcal{F}(1/2)$. According to our theory,

$$\mathcal{F}^\epsilon_{\text{num}}(x) = \mathcal{F}(x) + O(\epsilon). \tag{116}$$

Examples are given in Fig. 12 (we suppressed all indices on $\mathcal{F}$). The case $H = 0.33$ [Fig. 12(a)] corresponds to the plot in Fig. 10, with the same colors. One can clearly see that convergence in system size is slow for all H, but especially for the smaller ones. It becomes better for larger values of H.

We stopped our simulations after a total estimated 28 CPU years. The number of samples generated for each H and size is given in Fig. 11. As Eq. (115) indicates, we need more samples for small epsilon, i.e., H close to $H = 1/2$. It seems clear that measuring more than the curvature is illusory. We therefore defined

$$\gamma := \tfrac{1}{2}\partial_x^2 \mathcal{F}^\epsilon_{\text{num}}(x)|_{x=1/2} \tag{117}$$

and in practice measured it by fitting a polynomial of degree 2 in an x range from $x = 0.25$–0.75 for the smaller systems to $x = 0.15$–0.85 for the largest systems.

Analytically, we obtained in Eq. (74), with the Catalan constant C,

$$\gamma = 16(C-1) = 16\sum_{n=1}^{\infty}\frac{(-1)^n}{(2n+1)^2} \approx -1.344\,55. \tag{118}$$

Our direct numerical estimate for γ is shown in Fig. 3. One sees that extrapolation to $H = \frac{1}{2}$ is good only for large systems. An alternative and more precise way to extract γ is to define

$$\overline{\mathcal{F}}^\epsilon_{\text{num}}(x) := \tfrac{1}{2}\big[\mathcal{F}^\epsilon_{\text{num}}(x) + \mathcal{F}^{-\epsilon}_{\text{num}}(x)\big]. \tag{119}$$

This combination cancels the first subleading contribution in ϵ; the result is plotted in Fig. 13. Again one sees that $\mathcal{F}(x)$ is

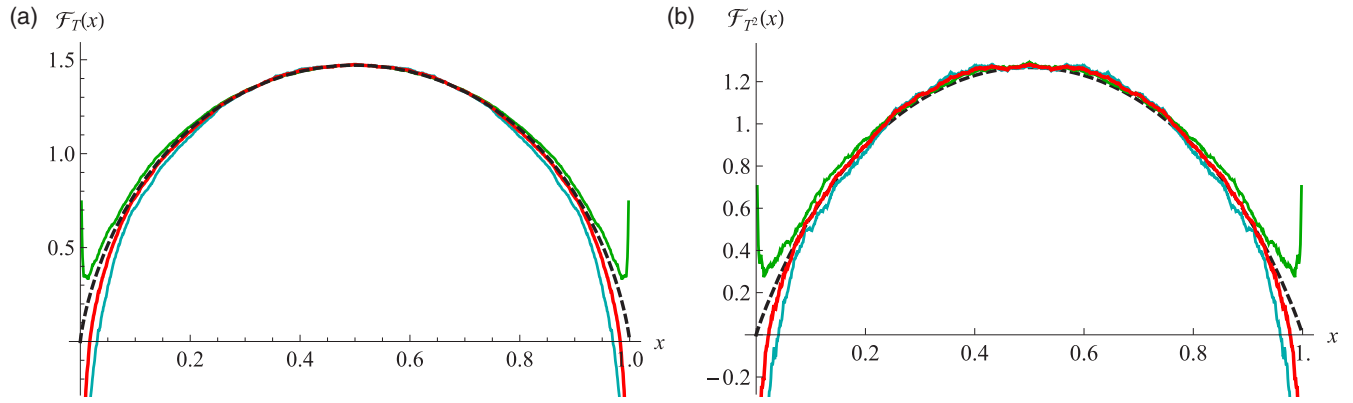

FIG. 14. (a) Mean (red) between the measured functions $\mathcal{F}_T(x)$ for $H = 0.45$ (dark cyan, bottom line) and $H = 0.55$ (dark green, top line). (b) Same as (a) but for $\mathcal{F}_{T^2}(x)$. The system size used is $N = 2^{24}$ and the total number of samples is 1.64×10^6 for $H = 0.45$ and 2.19×10^6 for $H = 0.55$.

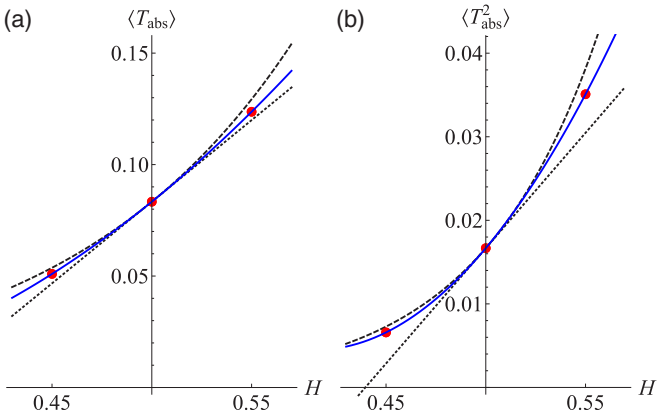

FIG. 15. (a) Mean, i.e., spatially averaged absorption time $\langle T_{\rm abs}\rangle = \int_0^1 dx \langle T_{\rm abs}(x)\rangle$. (b) Same as (a) but for the second moment. The black dotted line is the direct expansion in ϵ, which underestimates the true result. The dashed line is the exponentiation of this correction; it overestimates the result. The fit to a quadratic polynomial is given in Eqs. (121) and (122).

well approximated for large system sizes. Our best estimate is

$$\gamma_{\rm num} = -1.34 \pm 0.02. \tag{120}$$

C. Expectation of exit times and their squares

Let us now turn to the exit times as a function of x. Measurements of the scaling functions $\mathcal{F}_T(x)$ and $\mathcal{F}_{T^2}(x)$ given in Eq. (85) and Eqs. (89)–(90), respectively, are presented in Fig. 14 for $H = 0.45$ and $H = 0.55$. Their mean (in red) is a good approximation of the analytic curves (black dashed line). Simulations were performed for the largest system size at our disposal $N = 2^{24}$ and $H = 0.45$ and 0.55. Having generated a FBM, we put its starting position at x and then searched for the first instance when it was absorbed at either the upper or lower boundary. This procedure turned out to be rather time consuming, and we only evaluated this function about 2×10^6 times.

To estimate the spatially averaged first two moments of the exit times, we fitted their numerically obtained values, supplemented with the analytically known values for $H = 1/2$, with a polynomial of degree 2 in H. The result, shown in Fig. 15, is

$$\int_0^1 dx \langle T_{\rm exit}(x)\rangle = \frac{1}{12}[1 + 8.73\epsilon + 19.1\epsilon^2 + O(\epsilon^3)], \tag{121}$$

$$\int_0^1 dx \langle T^2_{\rm exit}(x)\rangle = \frac{1}{60}[1 + 17.1\epsilon + 100\epsilon^2 + O(\epsilon^3)]. \tag{122}$$

Comparison to Eqs. (95) and (103) yields excellent agreement for the first moment of the exit time (coefficient 8.758 to be compared to 8.73) and still very good agreement for the second moment (coefficient 16.563 as compared to 17.1). The latter is difficult to estimate, as higher-order corrections are seemingly large.

Let us finally mention that for $H = 1$, the probability that starting at x, the exit time is t, is given by

$$P^{H=1}_{\rm exit}(t|x) = \frac{1}{\sqrt{2\pi t^2}}\left[x e^{-x^2/2t^2} + (1-x) e^{-(1-x)^2/2t^2}\right]. \tag{123}$$

Averaging over x yields

$$\int_0^1 dx\, P^{H=1}_{\rm exit}(t|x) = \sqrt{\frac{2}{\pi}}\left[1 - e^{-1/2t^2}\right]. \tag{124}$$

All these distributions at $H = 1$ are pathologic. While they are normalizable, they have large tails which render already the first moment undefined. They are thus not a useful limit to test our formulas.

D. The time the span reaches 1

Our algorithm presented in Sec. V A to determine $P_1'(x)$ first determines the time the span (running maximum minus running minimum) reaches 1. For Brownian motion, its probability distribution was given in Eqs. (39) and (40). As we have seen in Sec. IV I, it gets corrected for $H \neq 1/2$, in a way we are currently unable to obtain analytically. The question we ask is how much it differs from the result for Brownian motion. The most important effect is a change in timescale,

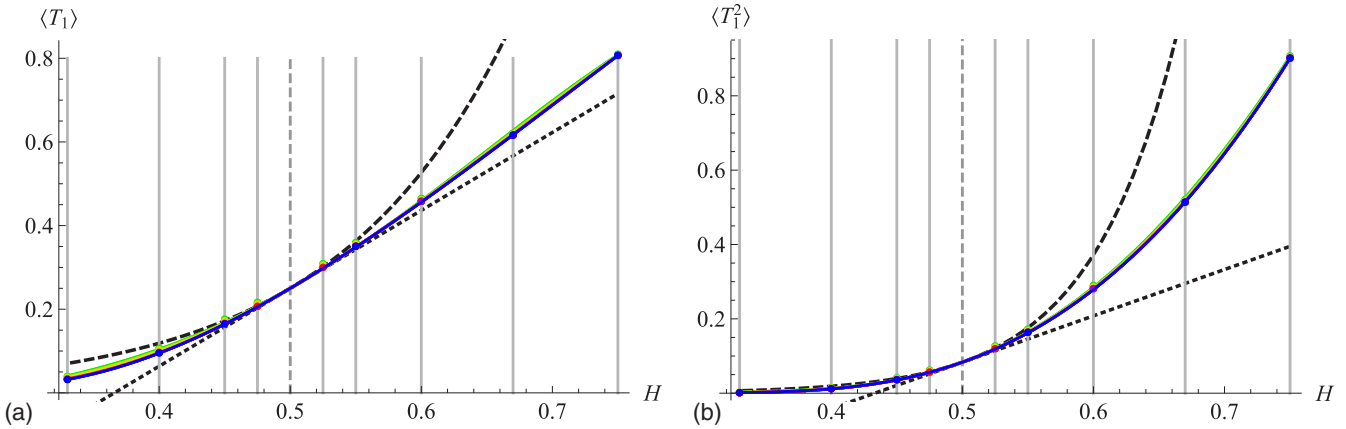

FIG. 16. (a) Expectation $\langle T_1\rangle$. The data points with interpolation follow the color code of Fig. 17. The black dotted line from Eq. (108) is the direct expansion in ϵ, which underestimates the numerical result, while its exponentiation given by the dashed line overestimates it. (b) Same as (a) but for $\langle T_1^2\rangle$, with the analytical result given in Eq. (109).

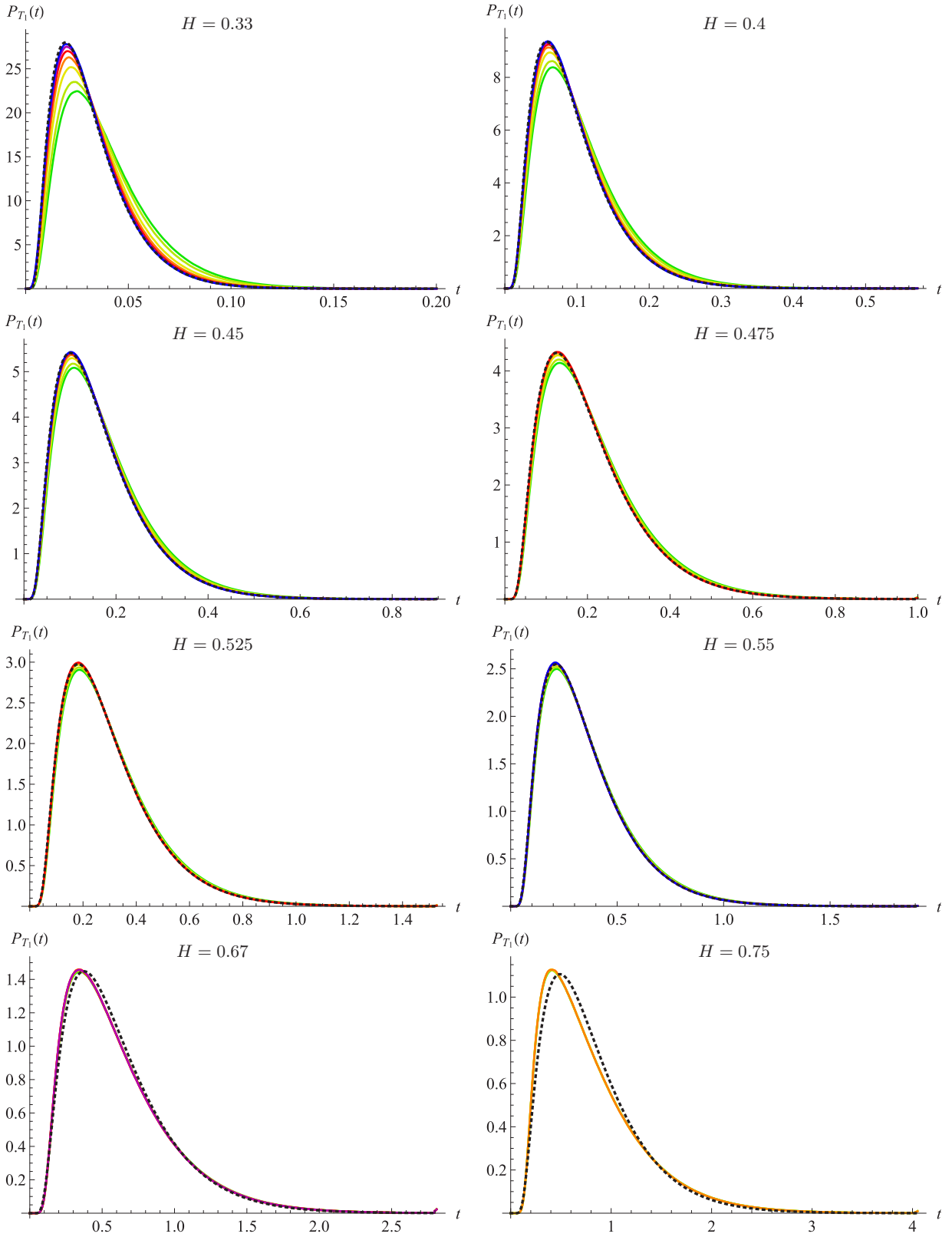

FIG. 17. Probability distribution of the numerically estimated time T_1 when the width of the process reaches 1, i.e., the process is absorbed irrespective of its starting position, for $N = 2^{13}$ (dark green), 2^{14} (green), 2^{16} (olive), 2^{18} (orange), 2^{20} (red), 2^{22} (dark magenta), and 2^{24} (blue). The characteristic time depends quite strongly on H. The result for $H = 1/2$ is between the distributions for $H = 0.475$ and $H = 0.525$. The black dotted line is the analytic result for $H = 1/2$, given in Eqs. (39)–(40), rescaled so that the first moment $\langle T_1 \rangle$ is correctly reproduced. Small systematic deviations are visible for small and large values of H, especially $H = 0.33$ and $H = 0.75$.

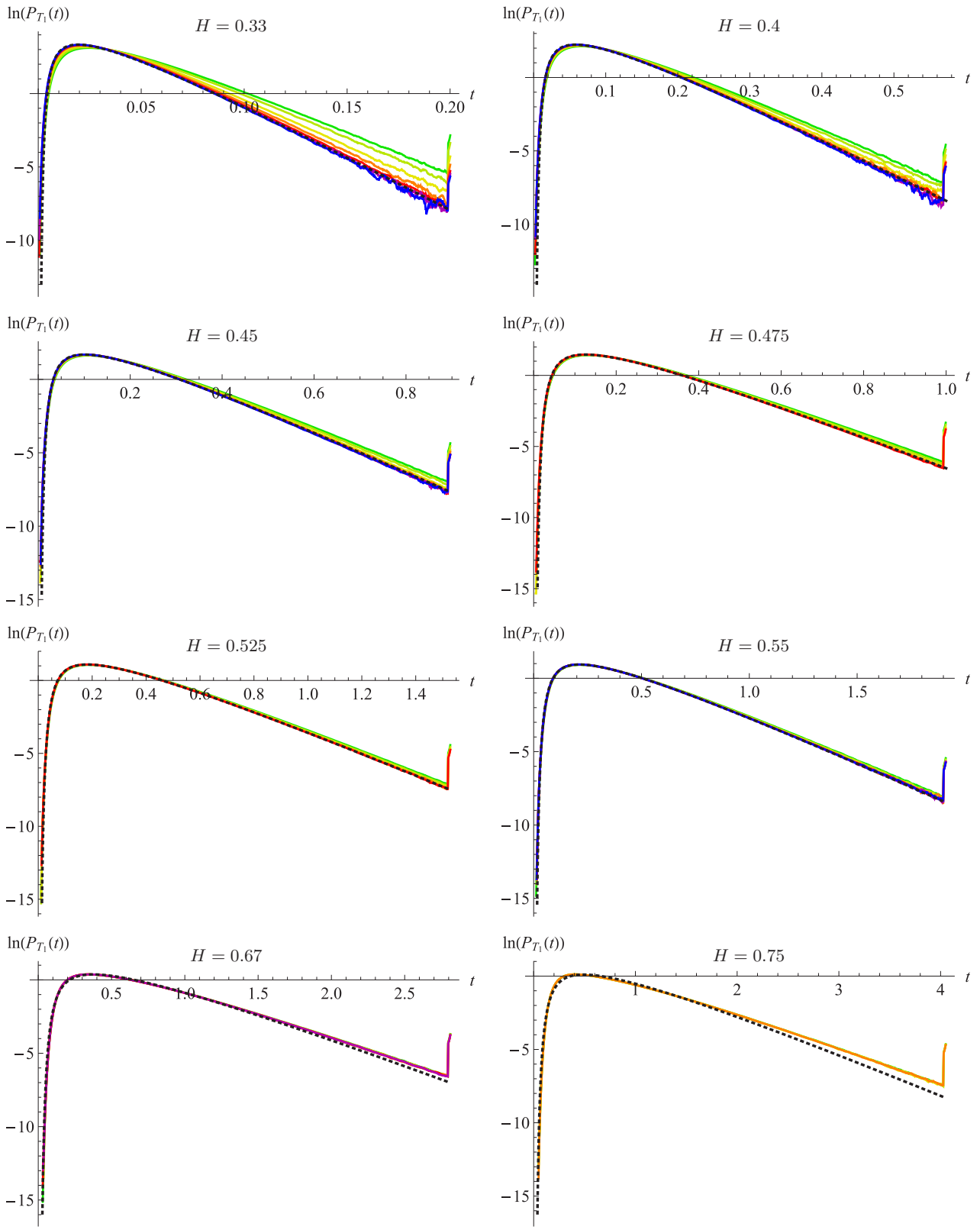

FIG. 18. Same as Fig. 17 but on a logarithmic scale. The little bump at large T corresponds to all realizations which did not exit up to that time, i.e., it is the integrated tail.

which we estimated in Eq. (108). Our numerical estimates, shown in Fig. 16, lead to

$$\langle T_1 \rangle = \tfrac{1}{4}[1 + 7.4\epsilon + 10.1\epsilon^2 - 18\epsilon^3 + \cdots], \quad (125)$$

$$\langle T_1^2 \rangle = \tfrac{1}{12}[1 + 15\epsilon + 75\epsilon^2 + 110\epsilon^3 + \cdots]. \quad (126)$$

This is in good agreement with Eqs. (108) and (109), where the order-ϵ coefficients read 7.45 and 14.96, respectively.

In order to compare the full distributions, we superimposed on the measured distribution the result for Brownian motion, rescaled such that the first moment $\langle T_1 \rangle$ is correctly reproduced. The result of this procedure is shown in Figs. 17 and 18. One can see deviations for large $|\epsilon|$, especially $H = 0.75$, which on the whole remain surprisingly small.

Finally, it is easy to show analytically that for $H = 1$,

$$P_{T_1}^{H=1}(t) = \sqrt{\frac{2}{\pi}} \frac{e^{-1/2t^2}}{t^2}. \quad (127)$$

Like the distributions (123) and (124), Eq. (127) has a large tail, leading to undefined moments.

E. Finite-discretization effects

As we saw in Fig. 10, there are important finite-discretization corrections. This is even more visible in Fig. 12, especially for $H = 0.33$ [Fig. 12(a)]. To better understand where this comes from, consider Fig. 9. In the given example, the width 1 is reached at $T_1 \approx 0.85$, with $x_0 \approx 0.58$. What is the error made, due to the finite discretization in time? Our argument will be made, as in the figure, for a particle trajectory exiting at the upper boundary, i.e., at t_* the running maximum $M_+(t)$ is growing, whereas the running minimum $M_-(t)$ is constant.The error in estimating the maximum is without consequences: While the true running maximum could be underestimated, this would only result in a slight underestimation of t_*. The problem in estimating $M_-(t)$ is more severe: If we underestimate the true minimum by δ, then x_0 is

$$x_0 = M_-(t) + \delta. \quad (128)$$

Denote by $P_N^{\text{miss}}(\delta)$ the distribution of δ. Close to the lower boundary, the probability at system size N, $P'_N(x)$, is

$$P'_{\text{N}}(x) = \int_0^\infty d\delta\, P_N^{\text{miss}}(\delta) P'_{N=\infty}(x - \delta). \quad (129)$$

The function $P_N^{\text{miss}}(\delta)$ should be a function of δ/τ^H, where $\tau = 1/N$, thus

$$P_N^{\text{miss}}(\delta) = P^{\text{miss}}(\delta N^H). \quad (130)$$

Transforming to Laplace variables, Eq. (129) now reads (with the tilde indicating the Laplace transform)

$$\tilde{P}'_N(\alpha) = \tilde{P}'_{N=\infty}(\alpha) \tilde{P}^{\text{miss}}(\alpha/N^H). \quad (131)$$

Taking a logarithm and rearranging yields

$$\ln(\tilde{P}'_{N=\infty}(\alpha)) = \ln(\tilde{P}'_N(\alpha)) - \ln(\tilde{P}^{\text{miss}}(\alpha/N^H)). \quad (132)$$

We currently have no theory for $\tilde{P}_{\text{miss}}(\alpha)$, but we find that a decent approximation for $H = 0.33$ is given by

$$\ln(\tilde{P}_{\text{miss}}(\alpha)) \approx 0.38 \ln(\tilde{P}_{\text{bridge}}(1.7\alpha)). \quad (133)$$

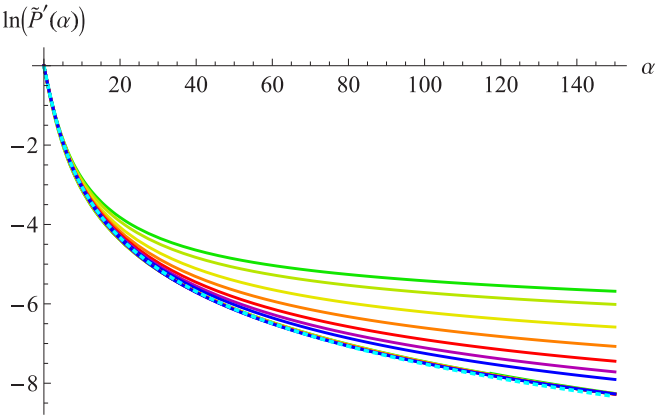

FIG. 19. The top seven curves are the logarithm of $\tilde{P}'(\alpha)$ [Laplace transform of $P'(x)$, as plotted in Fig. 10] for system sizes $N = 2^{13}$ (top, green) to $N = 2^{24}$ (blue). The lower solid curves are a scaling collapse of all seven curves, using Eqs. (132) and (133). The blue dashed line is the Laplace transform of the scaling ansatz (70), plotted in Fig. 10.

The function $P_{\text{bridge}}(m)$ is the maximum of a FBM bridge for duration $T = 1$, as given in Eq. (90) of Ref. [33]. Note that the numerical values of 0.38 and 1.7 are not significant (increasing one will decrease the other). As stated above, this formula is a guess, based on the following observations and hypothesis: Suppose that we measured a maximum m at time t, that the true maximum is between times t and $t + 1/N$, and that at time $t + 1/N$ the process again achieves its maximum (it should be smaller than the maximum). Then for Brownian motion the probability for the true maximum will be given by (133) with the numerical values set to 1. For a FBM, we again use the bridge process with the appropriate H. As for $H \neq 1/2$ the process is correlated, our ansatz induces a new error as it neglects correlations with the positions of the other points. The numbers induced above seem to compensate for the approximations made.

These arguments are illustrated in Fig. 19. The top seven curves show $\ln(\tilde{P}'_N(\alpha))$ for system sizes $N = 2^{13}$ (green, top) to $N = 2^{24}$ (blue, penultimate curve from the bottom). The remaining lower curve is a scaling collapse estimating $\ln(\tilde{P}'_{N=\infty}(\alpha))$, with $P_{\text{miss}}(\alpha)$ given in Eq. (133). The dashed line (cyan) is the Laplace transform of the scaling ansatz (70).

Our analysis shows that (i) discretization corrections are important, (ii) they come from an underestimation of the extension of the process on the side at which it does not exit, and (iii) there exists a correcting function one should be able to calculate analytically. The latter task is left for future research.

VI. CONCLUSION

In this article we considered the two-sided exit problem from a strip. We gave analytic results for the exit probabilities and times, in an expansion in $H - 1/2$. While our numerical simulations confirm our findings, they also point to a fundamental problem: If the observation of the underlying process is not done continuously but at a finite number of equally spaced times, the situation is exactly as in our numerical simulations. As a consequence, one may not see the predicted

analytic form and not even the correct scaling laws. It will be important to quantify these effects to properly interpret experimental data once they appear.

We also considered the probability distribution for the time the span (running maximum minus running mean), i.e., the area the process has visited, reaches 1. We gave analytic expressions of this probability for Brownian motion. For a FBM, evaluating corrections to its first moment analytically allows us to give a rather good approximation for this observable, without any adjustable parameter. Our results can be extended to include drift, and to one or two reflecting boundaries.

ACKNOWLEDGMENTS

It is a pleasure to thank Olivier Benichou, Mathieu Delorme, Alberto Rosso, Alejandro Kolton, Tridib Sadhu, and Sidney Redner for stimulating discussions and the two referees for their constructive remarks.

[1] W. Feller, *Introduction to Probability Theory and Its Applications* (Wiley, New York, 1950).
[2] S. Redner, *A Guide to First-Passage Problems* (Cambridge University Press, Cambridge, 2001).
[3] M. Muthukumar, Polymer translocation through a hole, J. Chem. Phys. **111**, 10371 (1999).
[4] D. K. Lubensky and D. R. Nelson, Driven polymer translocation through a narrow pore, Biophys. J. **77**, 1824 (1999).
[5] A. J. Storm, C. Storm, J. Chen, H. Zandbergen, J.-F. Joanny, and C. Dekker, Fast DNA translocation through a solid-state nanopore, Nano Lett. **5**, 1193 (2005).
[6] D. Panja and G. T. Barkema, Simulations of two-dimensional unbiased polymer translocation using the bond fluctuation model, J. Chem. Phys. **132**, 014902 (2010).
[7] D. Panja, G. T. Barkema, and R. C. Ball, Anomalous dynamics of unbiased polymer translocation through a narrow pore, J. Phys.: Condens. Matter **19**, 432202 (2007).
[8] A. Zoia, A. Rosso, and S. N. Majumdar, Asymptotic Behavior of Self-Affine Processes in Semi-Infinite Domains, Phys. Rev. Lett. **102**, 120602 (2009).
[9] B. B. Mandelbrot and J. W. Van Ness, Fractional Brownian motions, fractional noises and applications, SIAM Rev. **10**, 422 (1968).
[10] R. B. Davies and D. S. Harte, Tests for Hurst effect, Biometrika **74**, 95 (1987).
[11] A. B. Dieker, Simulation of fractional Brownian motion, Ph.D. thesis, University of Twente, 2004.
[12] A. B. Dieker and M. Mandjes, On spectral simulation of fractional Brownian motion, Probab. Eng. Inform. Sci. **17**, 417 (2003).
[13] L. Decreusefond and A. S. Üstünel, *ESAIM: Proceedings on Fractional Differential Systems: Models, Methods and Applications* (EDP Sciences, Les Ulis, 1998), Vol. 5, pp. 75–86.
[14] R. Metzler and J. Klafter, The random walk's guide to anomalous diffusion: A fractional dynamics approach, Phys. Rep. **339**, 1 (2000).
[15] P. L. Krapivsky, K. Mallick, and T. Sadhu, Dynamical properties of single-file diffusion, J. Stat. Mech. (2015) P09007.
[16] T. Sadhu and B. Derrida, Large deviation function of a tracer position in single file diffusion, J. Stat. Mech. (2015) P09008.
[17] T. Sadhu and B. Derrida, Correlations of the density and of the current in non-equilibrium diffusive systems, J. Stat. Mech. (2016) 113202.
[18] J. L. A. Dubbeldam, V. G. Rostiashvili, A. Milchev, and T. A. Vilgis, Fractional Brownian motion approach to polymer translocation: The governing equation of motion, Phys. Rev. E **83**, 011802 (2011).
[19] V. Palyulin, T. Ala-Nissila, and R. Metzler, Polymer translocation: The first two decades and the recent diversification, Soft Matter **10**, 9016 (2014).
[20] J.-P. Bouchaud and A. Georges, Anomalous diffusion in disordered media: Statistical mechanisms, models and physical applications, Phys. Rep. **195**, 127 (1990).
[21] N. J. Cutland, P. E. Kopp, and W. Willinger, in *Seminar on Stochastic Analysis, Random Fields and Applications*, edited by E. Bolthausen, M. Dozzi, and F. Russo, Progress in Probability Vol. 36 (Birkhäuser, Basel, 1995), pp. 327–351.
[22] T. Sottinen, Fractional Brownian motion, random walks and binary market models, Financ. Stoch. **5**, 343 (2001).
[23] B. B. Mandelbrot and J. R. Wallis, Noah, Joseph, and operational hydrology, Water Resour. Res. **4**, 909 (1968).
[24] S. Gupta, A. Rosso, and C. Texier, Dynamics of a Tagged Monomer: Effects of Elastic Pinning and Harmonic Absorption, Phys. Rev. Lett. **111**, 210601 (2013).
[25] E. Monte-Moreno and M. Hernández-Pajares, Occurrence of solar flares viewed with GPS: Statistics and fractal nature, J. Geophys. Res.: Space Phys. **119**, 9216 (2014).
[26] I. Simonsen, Measuring anti-correlations in the nordic electricity spot market by wavelets, Physica A **322**, 597 (2003).
[27] I. Norros, On the use of fractional Brownian motion in the theory of connectionless networks, IEEE J. Sel. Areas Commun. **13**, 953 (1995).
[28] K. Burnecki, E. Kepten, J. Janczura, I. Bronshtein, Y. Garini, and A. Weron, Universal algorithm for identification of fractional Brownian motion. A case of telomere subdiffusion, Biophys. J. **103**, 1839 (2012).
[29] D. Ernst, M. Hellmann, J. Kohler, and M. Weiss, Fractional Brownian motion in crowded fluids, Soft Matter **8**, 4886 (2012).
[30] K. J. Wiese, S. N. Majumdar, and A. Rosso, Perturbation theory for fractional Brownian motion in presence of absorbing boundaries, Phys. Rev. E **83**, 061141 (2011).
[31] M. Delorme and K. J. Wiese, Maximum of a Fractional Brownian Motion: Analytic Results from Perturbation Theory, Phys. Rev. Lett. **115**, 210601 (2015).
[32] M. Delorme, A. Rosso, and K. J. Wiese, Pickands' constant at first order in an expansion around Brownian motion, J. Phys. A: Math. Theor. **50**, 16LT04 (2017).
[33] M. Delorme and K. J. Wiese, Extreme-value statistics of fractional Brownian motion bridges, Phys. Rev. E **94**, 052105 (2016).
[34] M. Delorme and K. J. Wiese, Perturbative expansion for the maximum of fractional Brownian motion, Phys. Rev. E **94**, 012134 (2016).

[35] M. Delorme, Stochastic processes and disordered systems, around Brownian motion, Ph.D. thesis, PSL Research University, 2016.

[36] T. Sadhu, M. Delorme, and K. J. Wiese, Generalized Arcsine Laws for Fractional Brownian Motion, Phys. Rev. Lett. **120**, 040603 (2018).

[37] S. N. Majumdar, A. Rosso, and A. Zoia, Hitting Probability for Anomalous Diffusion Processes, Phys. Rev. Lett. **104**, 020602 (2010).

[38] S. N. Majumdar, Persistence in nonequilibrium systems, Curr. Sci. **77**, 370 (1999).

[39] H. E. Daniels, The probability distribution of the extent of a random chain, Math. Proc. Cambridge Philos. Soc. **37**, 244 (1941).

[40] W. Feller, The asymptotic distribution of the range of sums of independent random variables, Ann. Math. Statist. **22**, 427 (1951).

[41] G. H. Weiss and R. J. Rubin, The theory of ordered spans of unrestricted random walks, J. Stat. Phys. **14**, 333 (1976).

[42] V. Palleschi and M. R. Torquati, Mean first-passage time for random-walk span: Comparison between theory and numerical experiment, Phys. Rev. A **40**, 4685 (1989).

[43] T. Guérin, N. Levernier, O. Bénichou, and R. Voituriez, Mean first-passage times of non-Markovian random walkers in confinement, Nature (London) **534**, 356 (2016).